PERGAMON

Quaternary Science Reviews 22 (2003) 319–342

QSR

# A high resolution late Holocene palaeo environmental record from the central Adriatic Sea

F. Oldfield[a,*], A. Asioli[b], C.A. Accorsi[c], A.M. Mercuri[c], S. Juggins[d], L. Langone[e], T. Rolph[f], F. Trincardi[e], G. Wolff[g], Z. Gibbs[a], L. Vigliotti[e], M. Frignani[e], K. van der Post[a], N. Branch[h]

[a] *Department of Geography, University of Liverpool, Liverpool, L69 3BX, UK*
[b] *Istituto di Geoscienze e Georisorse del C.N.R.- sezione di Padova, c/o Dip. Mineralogia e Petrologia dell'Università di Padova, C.so Garibaldi, 37, 35137 Padova, Italy*
[c] *Orto Botanico, Via Caduti in Guerra 127, 41100 Modena, Italy*
[d] *Department of Geography, University of Newcastle, Newcastle upon Tyne, NE1 7RU, UK*
[e] *CNR Istituto per la Geologia Marina, Via Gobetti 101, 40129 Bologna, Italy*
[f] *Department of Geology, University of Newcastle, Callaghan 2308, NSW, Australia*
[g] *Department of Earth Sciences, University of Liverpool, Liverpool, L69 3BX, UK*
[h] *Department of Geography, Royal Holloway University of London, TW20 0EX, UK*

Received 4 July 2001; accepted 23 July 2002

**Abstract**

A multi-proxy study of a Holocene sediment core (RF 93-30) from the western flank of the central Adriatic, in 77 m of water, reveals a sequence of changes in terrestrial vegetation, terrigenous sediment input and benthic fauna, as well as evidence for variations in sea surface temperature spanning most of the last 7000 yr. The chronology of sedimentation is based on several lines of evidence, including AMS $^{14}C$ dates of foraminifera extracted from the core, palaeomagnetic secular variation, pollen indicators and dated tephra. The temporal resolution increases towards the surface and, for some of the properties measured, is sub-decadal for the last few centuries.

The main changes recorded in vegetation, sedimentation and benthic foraminiferal assemblages appear to be directly related to human activity in the sediment source area, which includes the Po valley and the eastern flanks of the central and northern Appenines. The most striking episodes of deforestation and expanding human impact begin around 3600 BP (Late Bronze Age) and 700 BP (Medieval) and each leads to an acceleration in mass sedimentation and an increase in the proportion of terrigenous material, reflecting the response of surface processes to widespread forest clearance and cultivation. Although human impact appears to be the proximal cause of these changes, climatic effects may also have been important. During these periods, signs of stress are detectable in the benthic foram morphotype assemblages. Between these two periods of increased terrigeneous sedimentation there is smaller peak in sedimentation rate around 2400BP which is not associated with evidence for deforestation, shifts in the balance between terrigenous and authigenic sedimentation, or changes in benthic foraminifera.

The mineral magnetic record provides a sensitive indicator of changing sediment sources: during forested periods of reduced terrigenous input it is dominated by authigenic bacterial magnetite, whereas during periods of increased erosion, anti-ferromagetic minerals (haematite and/or goethite) become more important, as well as both paramagnetic minerals and super-paramagnetic magnetite. Analysis of the alkenone, $U^{k'}_{37}$, record provides an indication of possible changes in sea surface temperature during the period, but it is premature to place too much reliance on these inferred changes until the indirect effects of past changes in the depth of the halocline and in circulation have been more fully evaluated.

The combination of methods used and the results obtained illustrate the potential value of such high resolution near-shore marine sedimentary sequences for recording wide-scale human impact, documenting the effects of this on marine sedimentation and fauna and, potentially, disentangling evidence for human activities from that for past changes in climate.


*Corresponding author. Fax: +44-0151-625-7418.
*E-mail address:* f.oldfield@btinternet.com (F. Oldfield).

0277-3791/03/$ - see front matter © 2002 Elsevier Science Ltd. All rights reserved.
PII: S 0 2 7 7 - 3 7 9 1 ( 0 2 ) 0 0 0 8 8 - 4

## 1. Introduction

Studies of marine sediment cores with the potential for sub-decadal temporal resolution are relatively rare outside the confines of periodically anoxic basins recording rapid sedimentation, estuarine or deltaic environments and some fiords. The Core studied (RF 93-30) is one of 11 Adriatic Cores incorporated in the PALICLAS project (Guilizzoni and Oldfield, 1996), spanning different periods, at varying levels of temporal resolution, from Oxygen Isotope Stage 4 to the present day. The range of techniques employed in the research on Core 93-30 includes radiometric dating using $^{14}C$, and $^{210}Pb$, C and N element determination, analysis of tephra, pollen, planktonic and benthic foraminifera, palaeomagnetic and rock-magnetic measurements and alkenone extraction and subsequent palaeo-temperature reconstruction. The aim of the research has been to provide a high-resolution record of human impact on some components of both terrestrial and marine ecosystems, especially for the last two millennia and to set alongside this some preliminary evidence for changing sea-surface temperature. By doing this, we hope to demonstrate the potential of this type of archive for linking continental and marine records, for disentangling signals of human impact from those reflecting climate variability and for exploring the interaction of these where both have been contributors to environmental change during the late Holocene. Preliminary accounts of some of the results presented here are outlined in various chapters in Guilizzoni and Oldfield (1996). Here we present all the results obtained so far and seek to develop an integrated assessment of their palaeo-environmental implications.

## 2. Core location and stratigraphic context

Core RF 93-30 (Lat. 42°40′01″N; Long. 15°40′03″E) is from the western flank of the Adriatic taken in 77 m of water. The core location is 18 km north of the north coast of the Gargano Promontory and a similar distance ESE of the Tremiti Islands (Fig. 1). It lies some 55 km SE of the centre of the Mid-Adriatic Depression from which other Holocene cores, IN 21-68 (Oldfield et al., 1995), IN 23-68 (Jorissen, 1988), CM 92-43 (Asioli et al., 1999, 2001) and PAL 94-66 (Guilizzoni and Oldfield, 1996) were taken. RF 93-30 comes from within the late Holocene mud wedge or ‘high stand systems tract’ (HST) as defined by Trincardi et al. (1994). The late Holocene deposits rest on a regional seismic reflector that marks the time of the maximum marine transgression at the culmination of the Holocene sea-level rise some 5–6 kyr BP. This surface is marked as ‘mfs’ in Fig. 2, which shows the line drawing of a seismic profile through the coring site. The core was 6.25 m long and reached below the base of the HST deposits. The high stand deposits sampled in RF 93-30 form part of a band of sediment shore-parallel in form, banked against the east coast of Italy from the Po delta southwards (Fig. 1, modified from Correggiari et al., 2001). On the Adriatic shelf the late Holocene HST consists of a coastal mud prism that accumulated rapidly under the influence of the Po and several minor Apennine rivers, over the last 5.5 k cal. yr or less (Correggiari et al., 1996; Trincardi et al., 1996a; Correggiari et al., 2001); the depo-centre of the late Holocene HST lies, on average, some 15 km from the coastline, is elongated in a shore-parallel direction and reaches a maximum thickness of 35 m (Fig. 1), so there is the potential in future to provide a significantly more expanded record than the one presented here. This mud prism has a flat and gently dipping (0.02°) sandy topset region (Fig. 2); the foreset region is muddy and dips in the order of 0.5° (locally up to 1°). The offlap break, separating topset and foreset strata (Fig. 2), occurs in water depths that become progressively deeper from north to south (a few meters in the Po delta front and as much as 35 m in the region surrounding the Gargano Promontory). This shore-parallel thickness distribution reflects the location of the sediment entry points on the western side of the basin (Trincardi et al., 1994), and the time-averaged effect of the cyclonic water circulation that affects the western side of the basin with a dominant southeastward component (Artegiani et al., 1997). Several coalescing sediment sources contribute to the development of the late Holocene deposits. These include small basins on the eastern slopes of the Apennines (with a total drainage area of $2.3 \times 10^4\,km^2$, a mean suspended load of $2.4 \times 10^{10}$ kg/yr, and a sediment yield exceeding $10^6\,kg/km^2/yr$) and the Po river (drainage area of $5.4 \times 10^4\,km^2$, mean suspended load of $1.5 \times 10^{10}$ kg/yr and sediment yield of $0.28 \times 10^6\,kg/km^2/yr$) draining the northern Apennines and the southern Alps (Frignani et al., 1992; Milliman and Syvitski, 1992; Bartolini et al., 1996).

The full stratigraphic context of this and other cores used in the PALICLAS project is given in Trincardi et al. (1996a, b) and further seismic-stratigraphic information can be found in Correggiari et al. (2001). Because of the dominant shore-parallel sediment dispersal and its location well down the transport path, core RF93-30 is in an ideal situation to reflect an integrated record of major changes in supply regime affecting the entire region, rather than fluctuations in local fluvial systems.

The late Holocene HST in the Adriatic region rests on the maximum flooding surface (mfs; Fig. 2), a regional surface that marks the time of maximum landward shift of the shoreline and corresponds to an interval of condensed deposition on the shelf centered around

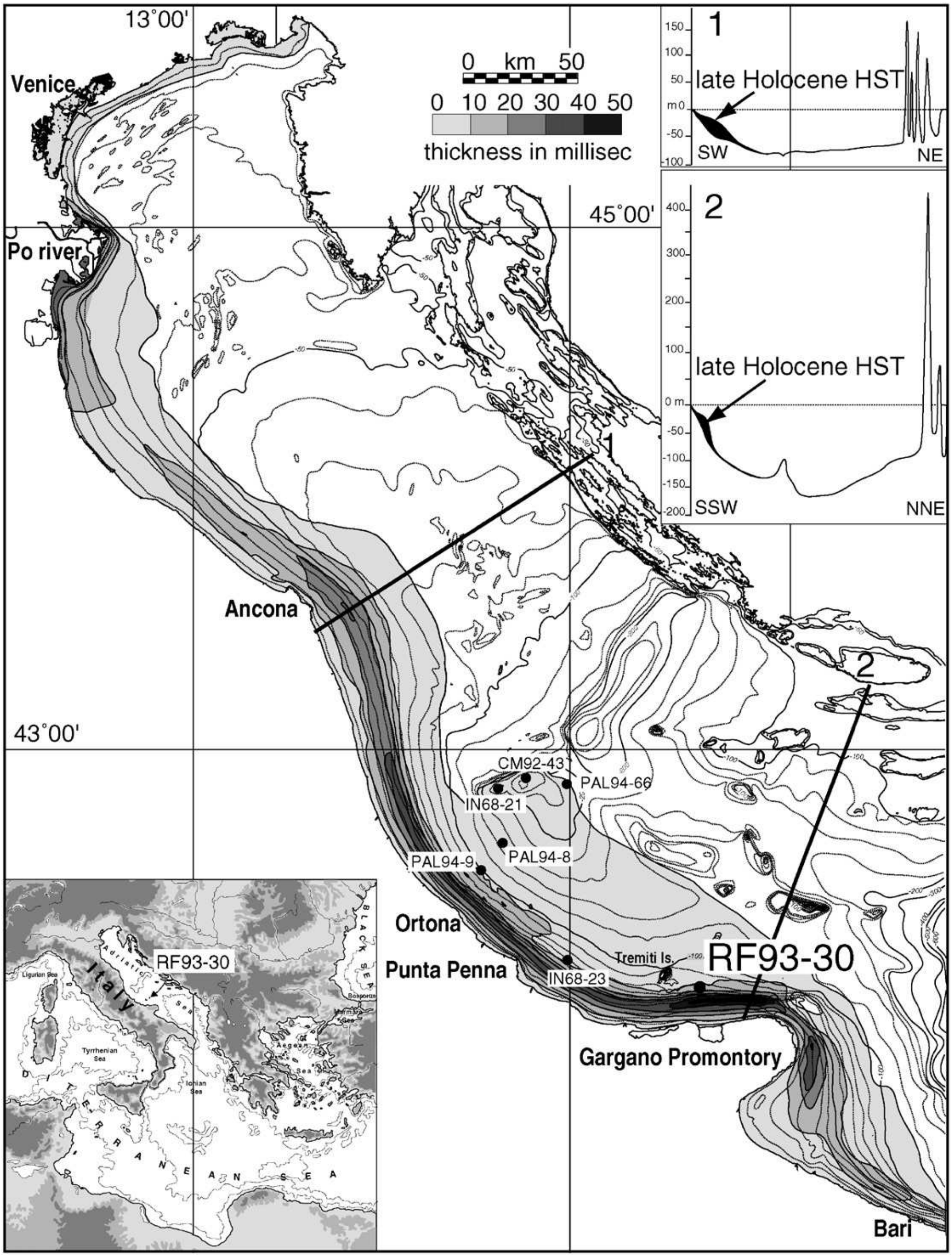


Fig. 1. Location map of Core RF 93-30, showing the relative thickness of the High Stand Systems Tract (HST) along the whole of the eastern flank of the Adriatic and its occurrence in two cross sections.

5.5 cal. kyr BP (Asioli, 1996; Correggiari et al., 1996; Trincardi et al., 1996a). In sections perpendicular to the coast, the late Holocene mud prism is composed of prograding sigmoids separated by high-amplitude reflectors, which correspond to minor flooding surfaces formed during short intervals of reduced deposition and/or enhanced reworking.

## 3. Methods

### 3.1. Seismic stratigraphy and coring

The seismic traces were obtained by means of a series of a digitally recorded, high-resolution seismic profiles using broad-band sound sources with firing rates

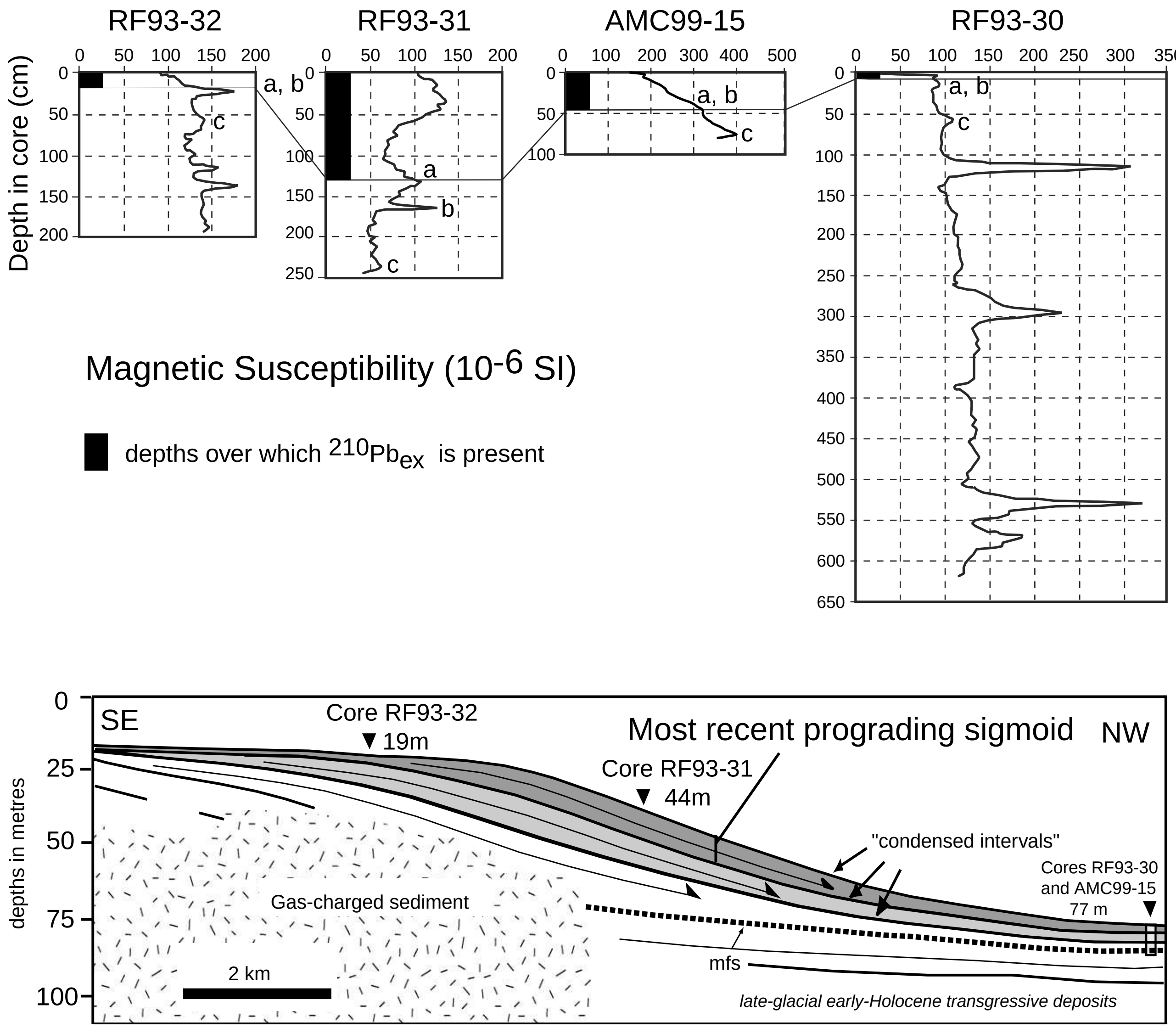


Fig. 2. The upper graphs show magnetic susceptibility plots for cores along a transect from the shore out to core RF 93-30, along with the depth to which excess (unsupported) $^{210}$Pb was detectable. The sketch of the seismic profile below outlines the geometry of the late Holocene sediments deposited subsequent to the full eustatic recovery of sea level (see text).

between 1/8 and 1/2 of a second. Typical pulse lengths of 1 or 2 ms allowed vertical resolution or the order of 50–100 cm. The core was obtained in 1993 using a 12 m long piston corer. After cutting into 1 m lengths, it was sliced vertically and stored at 4°C in the Istituto di Geologia Marina, Bologna. Only one half of the core was used for routine sub-sampling, though the 'archive' half eventually provided sub-samples for alkenone and tephra analysis.

### 3.2. Radiometric dating

The top 29 cm of the core were used for $^{210}$Pb analysis, using the alpha activity of the daughter isotope $^{210}$Po. The methods used are described in Frignani and Langone (1991) and the full results are given in Alvisi and Frignani (1996). Unsupported $^{210}$Pb is found in the top 5 cm of the core only, whereas in core AMC 99-15 taken subsequently at the same location, unsupported activity continues to almost 50 cm and in nearby core RF 93-31, which has similar surface activities, it continues to at least 90 cm (Fig. 2). These comparisons strongly suggests that sediment is missing from the top of RF 93-30, either as a result of a depositional hiatus or partial retrieval during coring.

Six AMS $^{14}$C dates were obtained on foraminifera at the Centre for Accelerator Mass Spectrometry of the Lawrence Livermore Laboratory, California. The calibrated ages shown in Table 1 were derived by applying the program CALIB 4.3 (Stuiver and Reimer, 1993) and the calibration dataset as in Stuiver et al. (1998). We chose the marine mixed curve and applied a constant

Table 1
Radiocarbon data from the Central Adriatic Sea

| Sample depth (cm) | $^{14}C$ age (yr BP) | Calibrated $^{14}C$ age range (yr BP) | Calibrated $^{14}C$ age (yr BP) | Material |
|---|---|---|---|---|
| RF93-30 | | | | |
| 127–131 | 1310±60 | 705–580 | 640±60 | Benthic foraminifera |
| 217–221 | 1860±60 | 1271–1123 | 1200±70 | Benthic foraminifera |
| 363–367 | 3150±60 | 2786–2591 | 2690±100 | Benthic foraminifera |
| 525–529 | 3960±60 | 3763–3562 | 3660±100 | Benthic foraminifera |
| 597–601 | 5970±50 | 6260–6081 | 6170±90 | Benthic foraminifera |
| 597–601 | 5880±60 | 6255–6086 | 6170±90 | Planktonic foraminifera |

Ages were calibrated using the program CALIB 4.3 (Stuiver and Reimer, 1993) and the calibration dataset as found by Stuiver et al. (1998). The marine mixed curve was chosen using delta reservoir ages of 137±28 and 220±50 yr for planktic and benthic foraminifera, respectively (Langone et al., 1996). The errors referred to are 1$\sigma$ (one sigma).

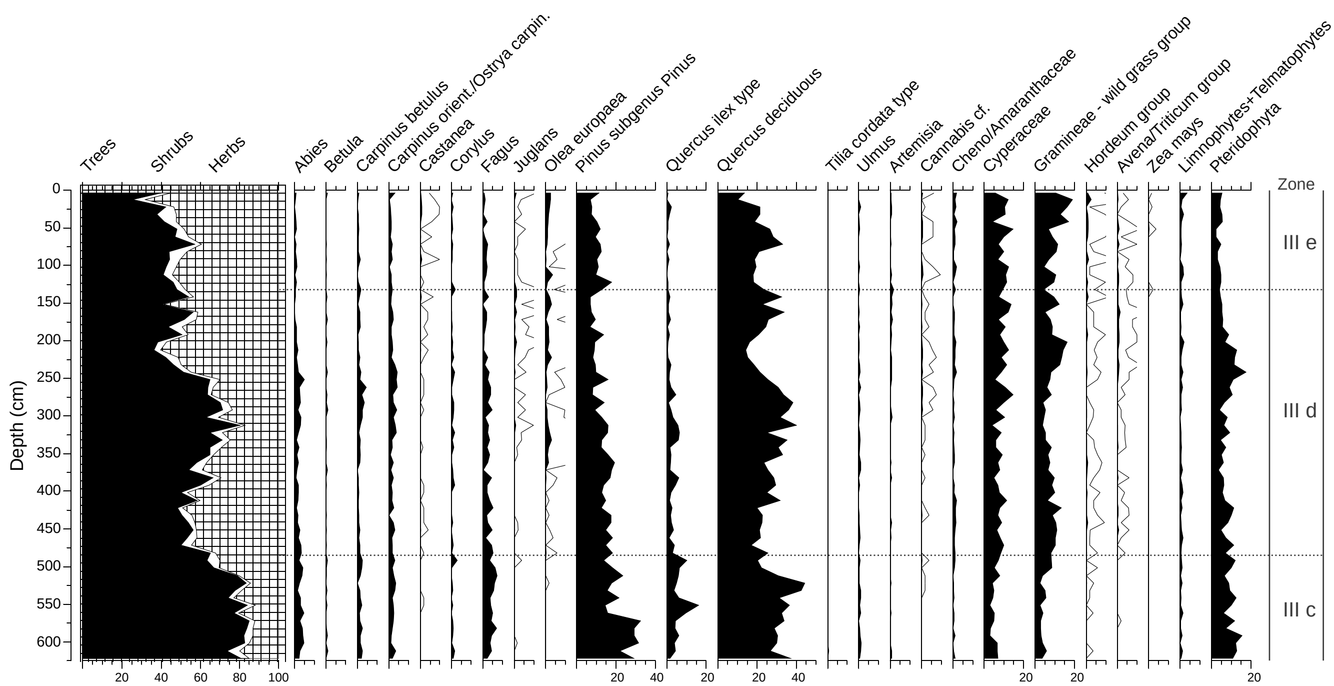


Fig. 3. Selected relative pollen frequencies as a percentage of the total pollen sum excluding *Pinus*.

reservoir age of 570±35 and 660±50 yr for planktonic and benthic foraminifera, respectively. The reservoir age of 570±35 yr for the planktonic foraminifera was determined by Langone et al. (1996) on the basis of multiple age determinations on a pre-bomb mollusc shell; the mollusc used for this purpose was a specimen of *Chlamys opercularis* collected alive in 1911 on the beach of Rimini in the North Adriatic. When using benthic foraminifera, a different reservoir age had to be taken into account. Paired dating on planktic and benthic foraminifera (*Uvigerina peregrina*) was done on level 597–601 cm of core RF93-30. A reservoir age of 660±50 yr was estimated by comparison between the two $^{14}C$ ages and was applied to all the dates obtained from benthic foraminifera. However, we recognize that the difference in the reservoir values of pelagic and benthic foraminifera may have varied over the last few thousand years as they did over the last 20 kyr (Langone et al., 1996). Moreover, part of the $^{14}C$-based chronology used in Langone et al. (1996) is in conflict with other lines of chronological evidence, hence with the age-depth model finally adopted here (see below).

### 3.3. Pollen analysis

Pollen samples were prepared using 10% Na-pyrophosphate, sieving at 200 μm, 10% HCl, acetolysis, heavy liquid separation (Na metatungstate hydrate of s.g.2.0) and centrifugation at 2000 rpm for 20 min (for details, see Lowe et al., 1996). Fig. 3 presents the pollen percentage results using pollen sums of 200–700 grains excluding *Pinus*, which is also excluded from the percentage calculations in view of its tendency to over-representation in marine sediments. Analyses were completed at 10 cm intervals from 10 cm to the base of the core.

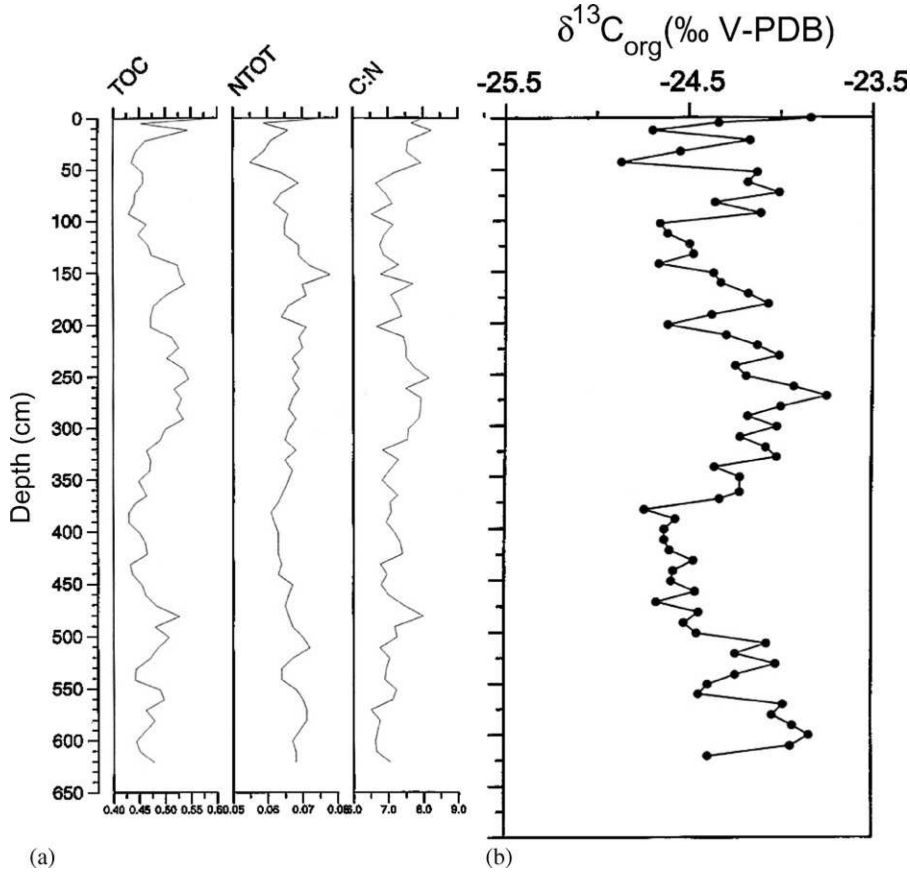


Fig. 4. Total organic carbon (TOC), total nitrogen (NTOT) and C:N ratio values are shown in (a). In (b), TOC values are plotted against $\delta^{13}C$ determinations.

### 3.4. Carbon and nitrogen analyses

Total organic carbon (TOC) and nitrogen were determined on 1 cm slices taken at 10 cm intervals down the whole core. Results (Fig. 4a) were obtained using a Fisons EA 1108 CHNS analyser after removal of the carbonate fraction by dissolution in HCl 1.5 N. The errors associated with the determinations are around 1% for carbon and 6% for nitrogen.

### 3.5. Stable isotopes

Stable isotopic analyses of organic C (Fig. 4b) were carried out using the Finnigan Delta Plus mass spectrometer, which was directly coupled to a Fisons NA2000 Elemental Analyser after acid treatment to eliminate the carbonate fraction. The IAEA standard NBS19 was used as calibration material. Uncertainties are lower than $\pm 0.2$‰, as determined from routine replicate measurements of a reference sample. Stable isotopic data are expressed in the conventional delta ($\delta$) notation in which the $^{13}C/^{12}C$ isotopic ratio is reported relative to the international PDB standard.

### 3.6. Magnetic measurements

After initial scanning for magnetic susceptibility variations (Trincardi et al., 1996a), 10 ml sub-samples of the uniformly clayey sediment were taken in plastic cubes for palaeomagnetic measurement. At this stage, the top 29 cm of the core were no longer available for study. The sample interval used left a 1 cm gap between each cube. Relative orientation was retained throughout, though the procedure was much more difficult in the upper part of the core, where the plastic nature of the sediment led to distortion as the cubes were inserted.

*NRM measurements* were undertaken using a Minispin slow speed spinner fluxgate magnetometer, both prior to AF-demagnetization and after partial demagnetization in an AF field of 30 mT. (Fig. 6).

*Rock-magnetic measurements* (Fig. 5) were volume based and included low field ($\kappa; \kappa_{LF}$) and frequency dependent ($\kappa_{fd}$) susceptibility measured using a Bartington MS 2 m, followed by Anhysteretic Remanent Magnetization (ARM) and subsequent, partial AF-demagnetization in a field of 30 mT, using a suitably modified Molspin AF-Demagnetizer.

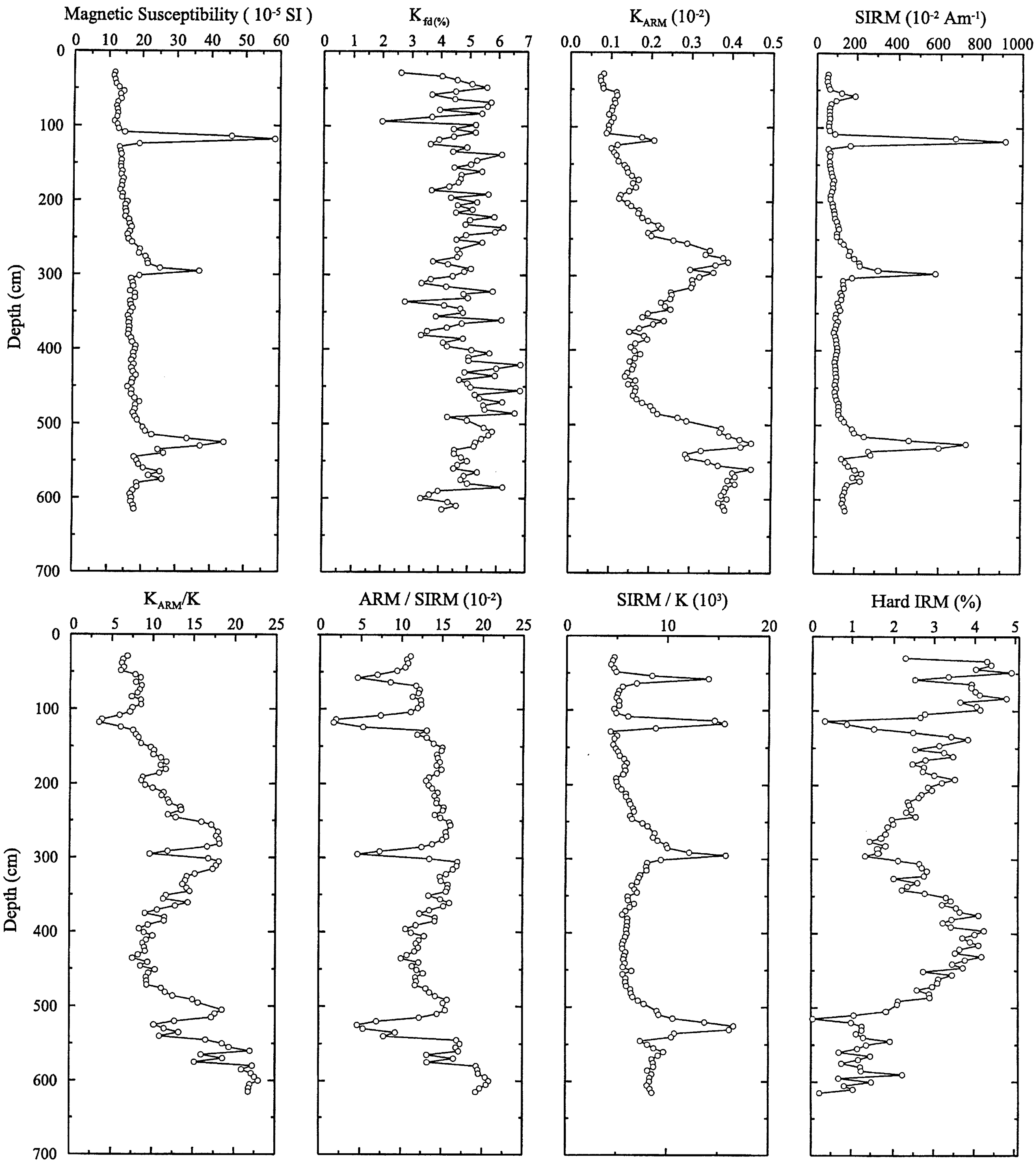


Fig. 5. Rock-magnetic properties, as defined in the text, plotted against depth. Note the three major spikes in concentration believed to relate to tephra layers: also the way in which (Hard)IRM % is inversely correlated with both ARM and the ARM-derived quotients. (Hard)IRM % is also directly correlated with relative intensity as shown in Fig. 6 (see text).

Samples were then given an Isothermal Remanent Magnetization in a field of 1 T (here designated SIRM) and subsequently demagnetized in back fields of −20, −40, −100 and −300 mT, using Molspin Pulse Magnetizers. All remanences were measured using a Minispin Magnetometer. The ARM values used in quotient calculations with susceptibility measurements are expressed as the susceptibility of ARM by normalizing the remanence to the strength of the DC bias field. In the case of volume based

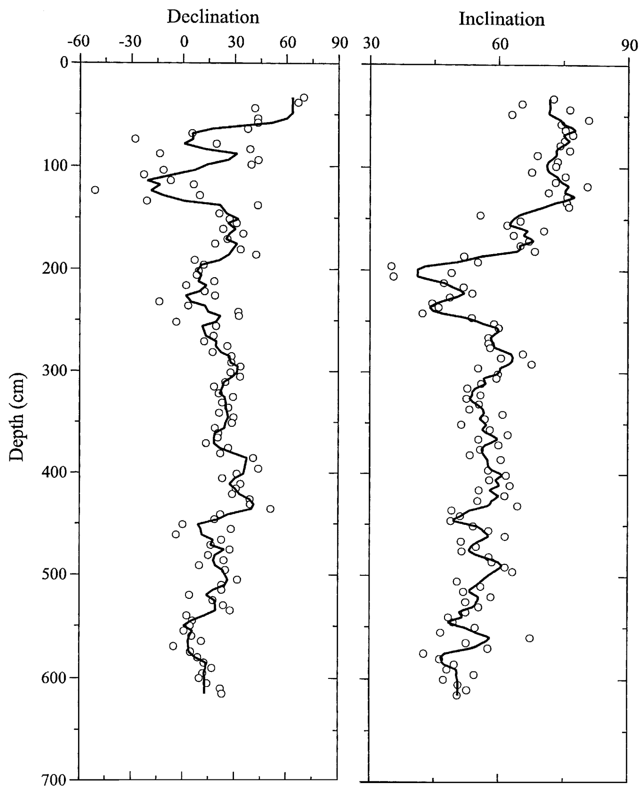


Fig. 6. The record of palaeosecular variation based on individual subsamples. Note the strong scatter, especially in declination values, in the upper part of the core where the sediment were more plastic.

measurements, as here, the resulting value is expressed as $\kappa_{ARM}$.

### 3.7. Transmission electron microscopy (TEM)

Subsamples from the lower part of the core were used for TEM imaging and grain identification, following the indications outlined in Oldfield (1994) that the typical Holocene sediments in the Adriatic were rich in bacterial magnetosomes. The magnetic extractions were carried out using the methods described in Hounslow and Maher (1996). The extracts obtained were examined in the Department of Material Sciences, University of Liverpool. A full account of the procedures used is given in Gibbs (2000). Typical TEM micrographs are reproduced in Fig. 7. The extraction efficiencies and counts of magnetosome types are summarized in Table 2.

### 3.8. Tephra

Sharp peaks in $\kappa$ and SIRM (Fig. 6) indicated the strong possibility of tephra layers. Samples from the depth spanning peaks at 510, 294, 116 and 55 cm were examined both optically (for glass shards) and geochemically, for comparison with major element composition of recorded tephra from the region (Calanchi et al., 1996; Turney, 1998; Davies et al., 2001).

### 3.9. Foraminiferal analysis

Extraction and counting of both planktonic and benthic foraminifera followed the methods outlined in Asioli (1996). Wherever possible, 300 planktonic and 300 benthic foraminifera were counted at each depth and normally at 10 cm intervals. Relative frequencies are expressed as percentages of the planktonic and benthic sums respectively and concentrations calculated as numbers per gram. The results are given in Fig. 8.

### 3.10. Alkenones (Fig. 9)

Sediments (5–7 g) were extracted by sonication ($\times$ 3) with dichloromethane (DCM)/methanol (3:1; 20 ml) after addition of an internal standard (2,21-dimethyldocosane). After centrifugation (3000 rpm; 15 min), the extracts were decanted and combined prior to removal of the solvent in vacuo. The total lipid extract was redissolved in the minimum volume of DCM and transferred to a small column (Pasteur pipette) containing anhydrous sodium sulphate and eluted with DCM (4 ml). The solvent was removed under a stream of nitrogen. Initial gas chromatography-mass spectrometry (GC-MS) analyses were then performed on the derivatised total extracts (*bis*-trimethylsilyltrifluoroacetamide; BSFTA, 1% trimethylsilyl chloride; 50 μl; 50°C; 30) min under conditions described previously (Kiriakouslakis et al., 2001).

$U^{k'}_{37}$ data were determined by quantification of the relative abundances of the $C_{37}$ di- and tri-unsaturated ketones ($C_{37:2}$ and $C_{37:3}$, respectively; Rechka and Maxwell, 1988) using chemical ionization GC-MS with ammonia as the reagent gas (Rosell-Mélé et al., 1995). Analyses were performed using the VG TS-250 mass spectrometer, as above. Conditions differed somewhat in that the samples were injected using a splitless injection system (325°C) onto the fused high temperature silica column (see above). The oven temperature was programmed from 180°C to 330°C at 6°C min$^{-1}$ and held for 10 min. Typical GC-MS conditions were ionization potential 70 eV; source temperature 170°C; trap current 400 μA and multiplier gain 390 V. The instrument was cycled every second in selected ion mode ($m/z$ 120, 230, 546, 547, 548, 549) and data were collected and processed as above. Peak areas for the di and tri-unsaturated $C_{37}$ ketones were corrected according to response factors determined by analysis of equimolar amounts of authentic standards (Rechka

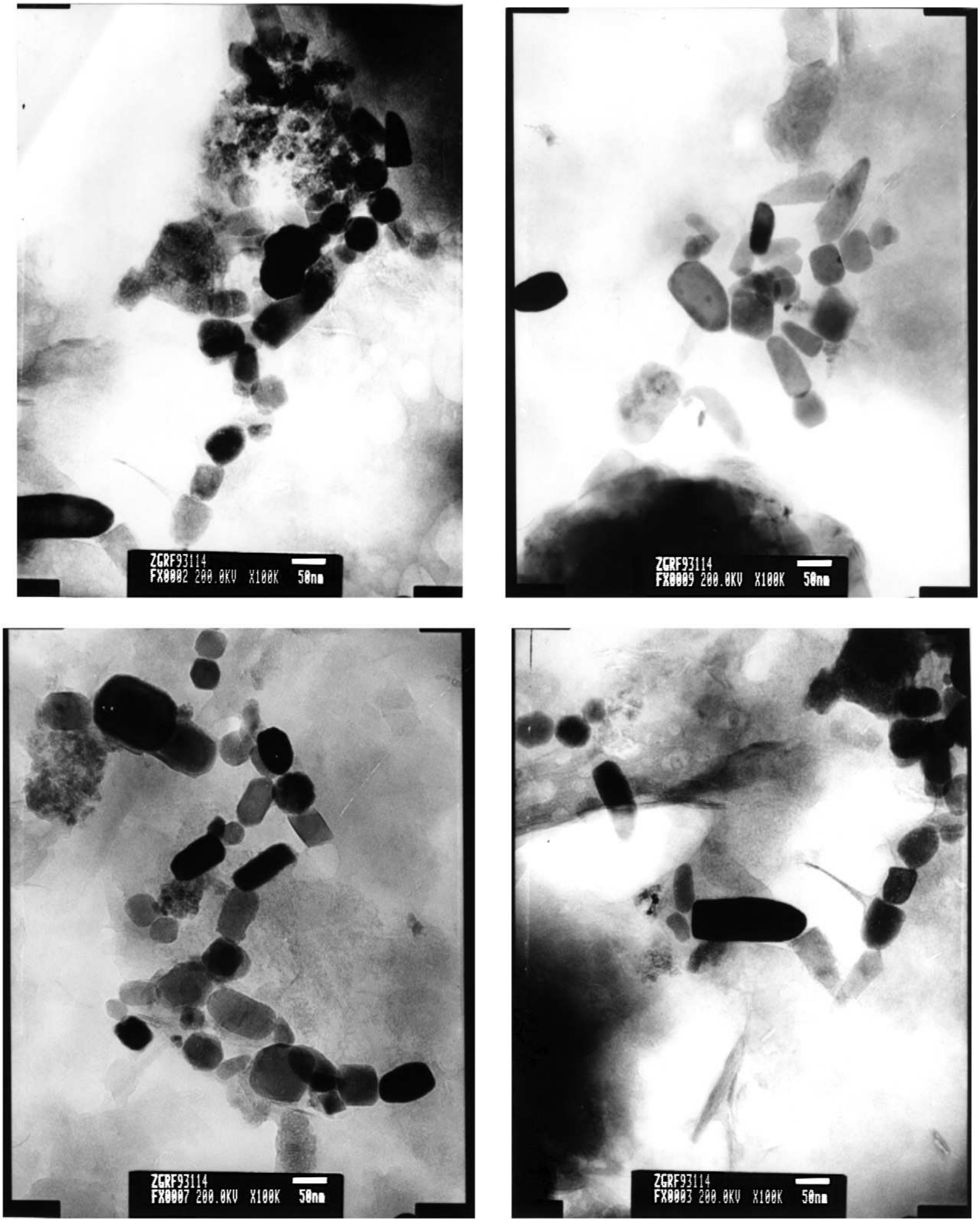


Fig. 7. TEM images of bacterial magnetosomes from the sediments below 500 cm. The photographs show the range of morphologies for which relative contributions are quantified in Table 2.

and Maxwell, 1988). The tetraunsaturated compound was not quantified, as full data GCMS analyses indicated that it was not present in detectable amounts in any of the samples.

The $U^{k'}_{37}$ was calculated according to the standard equation (Brassell et al., 1986):

$$U^{K'}_{37} = [C_{37:2}]/[C_{37:2} + C_{37:3}]. \tag{1}$$

Table 2
Transmission electron microscopy on magnetic extracts from Core RF 93-30. Summary of extraction efficiencies, grain counts and magnetosome morphologies

| Sample depths | ARM extraction efficiency (%) | SIRM extraction efficiency (%) | $\chi$ extraction efficiency (%) | Total grain count (No.) | % Biogenic magnetosomes (%) | % Non-biogenic grains (%) | Magnetosome morphologies (%) | | | |
|---|---|---|---|---|---|---|---|---|---|---|
| | | | | | | | *Hexagonal* | *Parallelepiped* | *Cubic* | *Bullet* |
| 565 cm | 0 | 17 | 45 | 170 | 75 | 25 | 29 | 34 | 3 | 34 |
| 570 cm | 33 | 36 | 23 | 2147 | 76 | 24 | 12 | 61 | 3 | 24 |
| 575 cm | 29 | 25 | 24 | 1066 | 85 | 15 | 14 | 60 | 10 | 16 |
| 580 cm | 58 | 54 | 59 | 515 | 53 | 47 | 36 | 27 | 13 | 25 |

## 4. Results

### 4.1. Pollen analysis (Fig. 3)

Pollen zones and sub-zones correlated with the scheme defined for Adriatic Core PAL 94-8 in Lowe et al. (1996) were defined as follows.

Sub-zone IIIc (623–485 cm). This sub-zone has the highest percentages of arboreal pollen (up to 80%) with the dominant taxon being deciduous *Quercus.* Other important tree taxa include *Quercus ilex* type, *Fagus* and *Pinus.* Poaceae (including cereal type) values are low and *Castanea*, *Juglans* and *Olea* are present only sporadically.

Sub-zone IIId (485–132 cm). There is a significant reduction, subsequent recovery and second reduction in arboreal pollen percentages in this sub-zone. *Olea* pollen, and subsequently *Castanea* and *Juglans* pollen become more abundant, or increase in the later part of the sub-zone. Pollen of cereals and ruderals becomes more abundant and the record of their presence more continuous.

Sub-zone IIIe (132–3 cm). The base of this sub-zone is marked by the first record of *Zea mays* pollen, as well as increased values for the *Hordeum* and *Avena-Triticum* groups.

### 4.2. Carbon and nitrogen analyses (Fig. 4)

Carbon values remain close to 0.5% and nitrogen values between 0.06% and 0.08% throughout the core. There is relatively close co-variance between the two elements and the C:N ratio is close to 7 save above 50 cm, where the values of both concentrations and of the ratio increase slightly towards the surface. This reflects early organic matter diagenesis below the sediment-water interface. $\delta^{13}C$ values range between −24.87‰ and −23.75‰, with a mean value of −24.30‰. Faganeli et al. (1994) constructed a mixing model for the determination of marine and terrestrial contributions to sedimentary organic matter using the $\delta^{13}C$ values of different end-members, i.e. phytoplanktonic ($\delta^{13}C = -21.0$‰) and riverine organic matter ($\delta^{13}C = -28.0$‰) in the Adriatic area. Because the TOC and carbon stable isotope curves are correlated, temperature and differences in plankton species composition are unlikely to be the main influences driving the isotopic fractionation of organic carbon in the Adriatic Sea (Faganeli et al., 1994). Using this model, a value of −24.5‰ means that the organic fraction is constituted by 50% of marine and 50% of terrestrial origin, though these estimates should be viewed with caution as the mean value for marine organic matter proposed by Farinelli is low compared with the range proposed for other coastal seas. Irrespective of the value chosen, the graph of $\delta^{13}C$ documents intervals of increased marine

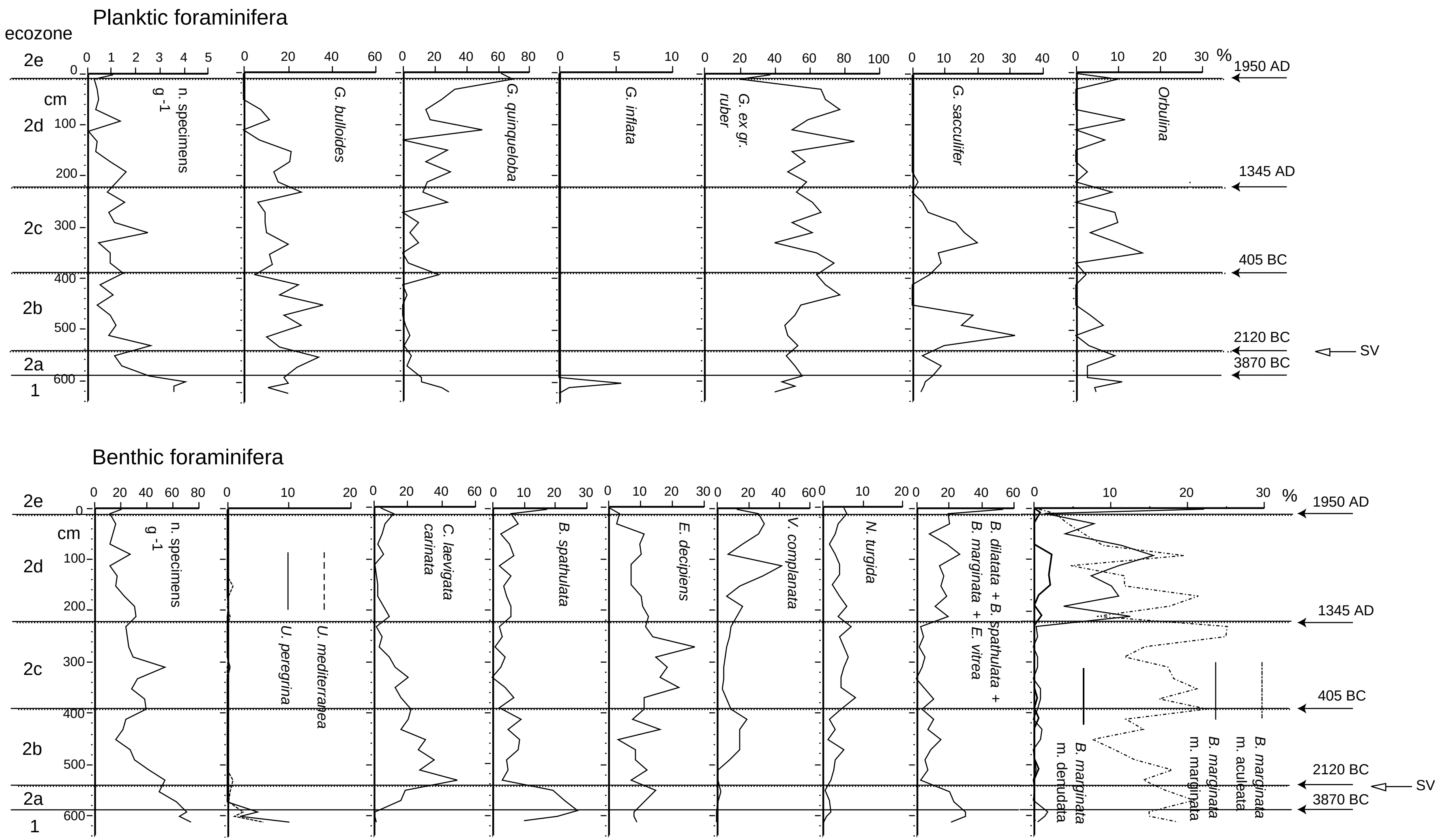


Fig. 8. Percentage values for planktonic (a) and benthic (b) foraminifera plotted against the ecozones defined in the text.

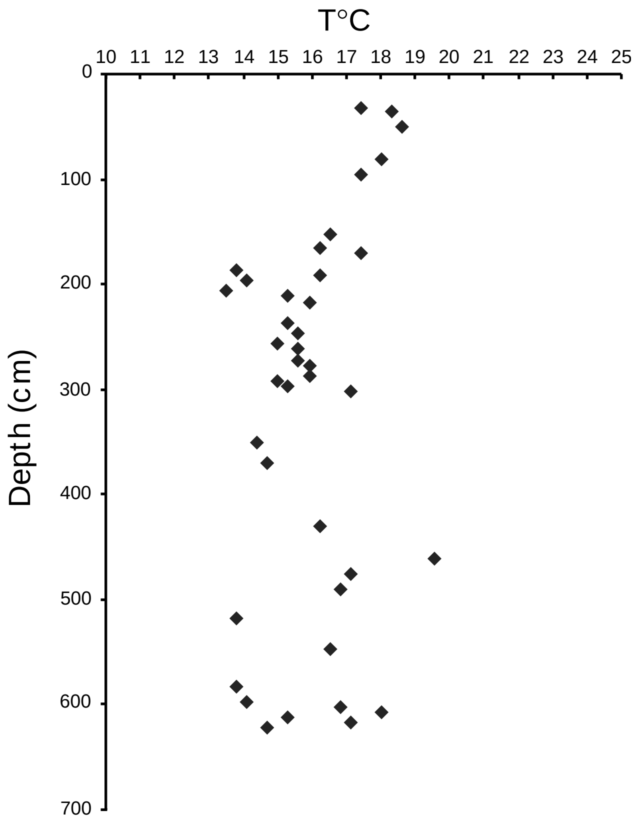


Fig. 9. Results of alkenone ($U^{k'}_{37}$) analyses converted to SSTs using the methods described in the text.

influence on the formation of organic matter (e.g. around 1000 yr BP; and during the early Bronze Age, the period corresponding the maximum flooding surface), and intervals of predominantly continental sources (e.g., the Late Bronze Age and Iron Age and during discreet episodes within the last 700 yr).

### *4.3. Magnetic measurements (Figs. 5 and 6)*

#### *4.3.1. Bulk magnetic parameters (Fig. 5)*

(1) SIRM and $\kappa_{LF}$. Both parameters clearly show the presence of three intervals with greatly enhanced values. The lowest (centred at 525–530 cm) has been confirmed as the "Avellino" tephra from Somma-Vesuvius and dated to ca 3660 cal BP. By association the peaks at 294 and 116 cm were also evaluated as possible tephra (see chronology section below), as well as the smaller spike in SIRM between 55 and 60 cm. Other variations in these concentration parameters are rather subdued.

(2) ARM. The ARM record also shows peaks corresponding to the three main SIRM spikes but only the youngest stands out clearly from the local background variations. The higher values associated with the lower two SIRM spikes are partly obscured by increased ARM values not associated with the SIRM maxima.

#### *4.3.2. Magnetic percentage and quotient values (Fig. 5)*

(1) Hard IRM % (% of SIRM with a coercivity greater than 300 mT). The three main SIRM peaks are associated with minima in Hard IRM. There are more gradual variations in this parameter which are essentially the inverse of those seen in the ARM record.

(2) $\kappa_{fd}$ (%). The frequency dependent susceptibility record shows little structure that can be related to variations in the bulk magnetic parameters. Most variation is essentially at the sample to sample level and therefore indicates that measurement noise is important and is superimposed on a background level which varies little from an average of close to 4%. The highest mean values correspond with the dip in ARM values and a peak in hard IRM between ca 400 and 480 cm. The lowest values are at the base of the core and around 250–400 cm. In the first case, they correspond with a maximum in ARM/SIRM, in the second case with a marked increase in ARM and ARM/SIRM. In both cases, the low values correspond with minima in hard IRM.

(3) $\kappa_{ARM}/\kappa_{LF}$ and ARM/SIRM. All the SIRM spikes show distinct minima in each quotient; this is true of the upper feature in the $\kappa_{ARM}/\kappa_{LF}$ and ARM/SIRM record. However there is some difference in the behaviour of the two quotients above and below ca 300 cm. Below, both records show a similar pattern of variation to that displayed by the ARM record while above 250 cm the general decrease is only clear in the $\kappa_{ARM}/\kappa_{LF}$ record.

(4) SIRM/$\kappa_{LF}$. In this record the SIRM spikes give rise to distinct narrow, well-defined maxima. The uppermost feature is especially strongly marked in the SIRM/$\kappa_{LF}$ quotient, which reaches values of a similar magnitude to those in the confidently identified tephra.

#### *4.3.3. Declination (Fig. 6)*

At depths above 150 cm, where subsampling was most affected by plastic distortion during insertion of the cubes, the declination record shows considerable scatter and furthermore indicates an unrealistically large easterly swing towards the top of the record. Below 150 cm the record shows a considerably reduced amplitude which never exceeds $\pm 30°$.

#### *4.3.4. Inclination (Fig. 6)*

The inclination record shows a distinct change in behaviour in a zone centred at a depth of 200 cm; the background value changes from $\sim 55°$ below to $\sim 75°$ above this zone while within the zone the inclination record reaches its lowest values.

#### *4.3.5. Relative intensity (Fig. 6)*

The relative intensity record is provided by the ratio of the partially demagnetized (30 mT) NRM and ARM. Above 250 cm this ratio shows considerable scatter which produces a number of short wavelength/high amplitude fluctuations. These are thought to be artefacts of the sampling problems already referred to above. Below this level the scatter is considerably reduced and the record shows a broad maximum between 340 and 500 cm. However a consideration of both the Hard IRM and ARM records indicates a correlation between the relative intensity and both of these bulk magnetic parameters; in the former case it is direct, in the latter an inverse correlation. This means that true changes in magnetic field intensity cannot be separated from mineral magnetic changes interpreted below as likely to be mainly the result of human activity. The record cannot therefore be regarded as a valid reflection of changes in geomagnetic intensity.

### 4.4. TEM analysis of magnetic extracts (Fig. 7 and Table 2)

All four samples used for magnetic extraction and TEM analysis were from the sediments between 565 and 585 cm, below the Avellino tephra, since the main aim was to establish the extent to which magnetosomes dominated the magnetic record during the period when evidence for human impact and erosion was minimal. Extraction efficiencies were determined using three magnetic parameters ARM, indicative of the proportion of finer grained ferrimagnets removed through extraction and $\chi$ and SIRM which indicate the changes in the concentration of the ferrimagnetic minerals within each sample. The extraction efficiencies varied between 17% and 59% (Table 2) with the best efficiencies recorded for sample 116. The poor ARM extraction efficiencies indicate that the data should be interpreted with a degree of caution as it can be argued that the extracts obtained are unlikely to be truly representative of the type and proportions of fine grained ferrimagnetic minerals present within a sample. However despite the variation in the extraction efficiencies between the samples all consistently point to the dominance of fine grained bacterial magnetosomes with grain counts ranging from 53% for sample 116 which had the best ARM extraction efficiency to 85% in sample 115 which had a significantly reduced ARM extraction efficiency of 29%.

The extracts contained a range of magnetosome morphologies (Table 2). The dominant morphology was the parallelepiped with the exception of sample 116 where the hexagonal morphology dominated. The cubic morphology was the least common in all samples.

### 4.5. Tephra analysis

Only the basal magnetic concentration peak at 525–530 cm has been independently confirmed as a tephra (Calanchi et al., 1996). Sediments from the magnetic 'spikes' at 55, 116 and 294 cm were subsequently re-examined in the Palaeoecology Laboratory, Queens University, Belfast, but without conclusive visual and geochemical confirmation of the presence of tephra (V. Hall, pers. comm.). Finally, sediments containing the SIRM peaks at 294 and 116 cm were processed using the techniques outlined in Turney (1998) and Davies et al. (2001), but again, no evidence for tephra was found.

### 4.6. Planktonic foraminifera (Fig. 8a)

Planktonic foraminifera are scarce; only the lowermost interval between 620 and 590 cm displays a relatively rich assemblage. The number of specimens is very low from 590 cm up to the top. Within this later interval, two major peaks are present at 530 and 300 cm. On the basis of the planktonic foraminifera, the core can be divided into three intervals.

620–590 cm: presence of *Globorotalia inflata* and *Globigerinoides ex gr. ruber*. *Globigerina bulloides*, *Globigerina quinqueloba* and *Orbulina* are also present.

580–220 cm: the number of total planktonic foraminifera decreases. *G. inflata* disappears while *Globigerinoides sacculifer* is present, peaking at 510 and 330 cm.

210–0 cm: *G. sacculifer* disappears. The assemblage, very impoverished, is mainly composed of *G. ex gr. ruber*. *G. quinqueloba* shows an increasing trend above 250 cm.

The available $^{14}C$ dates allow correlation of the interval at the base of which *G. inflata* disappears to ecozone 2 of the biostratigraphy proposed by Asioli (1996) for the Central Adriatic.

### 4.7. Benthic foraminifera (Fig. 8b)

To detect the environmental changes, it was necessary to consider the intraspecific variability that several species display. *Bulimina ex gr. marginata* displays the highest variability and several morphotypes were separated within this species. Using the criteria in Jorissen (1988), Van der Zwaan and Jorissen (1991) and Barmawidjaja et al. (1992), the following morphotypical populations may be recognized in the present core.

*B. marginata* morph aculeata: undercut absent, reduced and irregular ornamentation located at the younger part of the twisted test.

*B. marginata* morph denudata: the undercut is present but rounded.

*B. marginata* morph marginata: undercut well developed, spines aligned along the margin of each chamber.

The number of the benthic foraminifera is relatively high (70 specimens per gram of dried sediment) at the base of the core, then it decreases up to 450 cm where it reaches a minimum value of 20 specimens per gram. From 450 cm up to the top the number of specimens is between 20 and 30 per gram peaking at 31 cm.

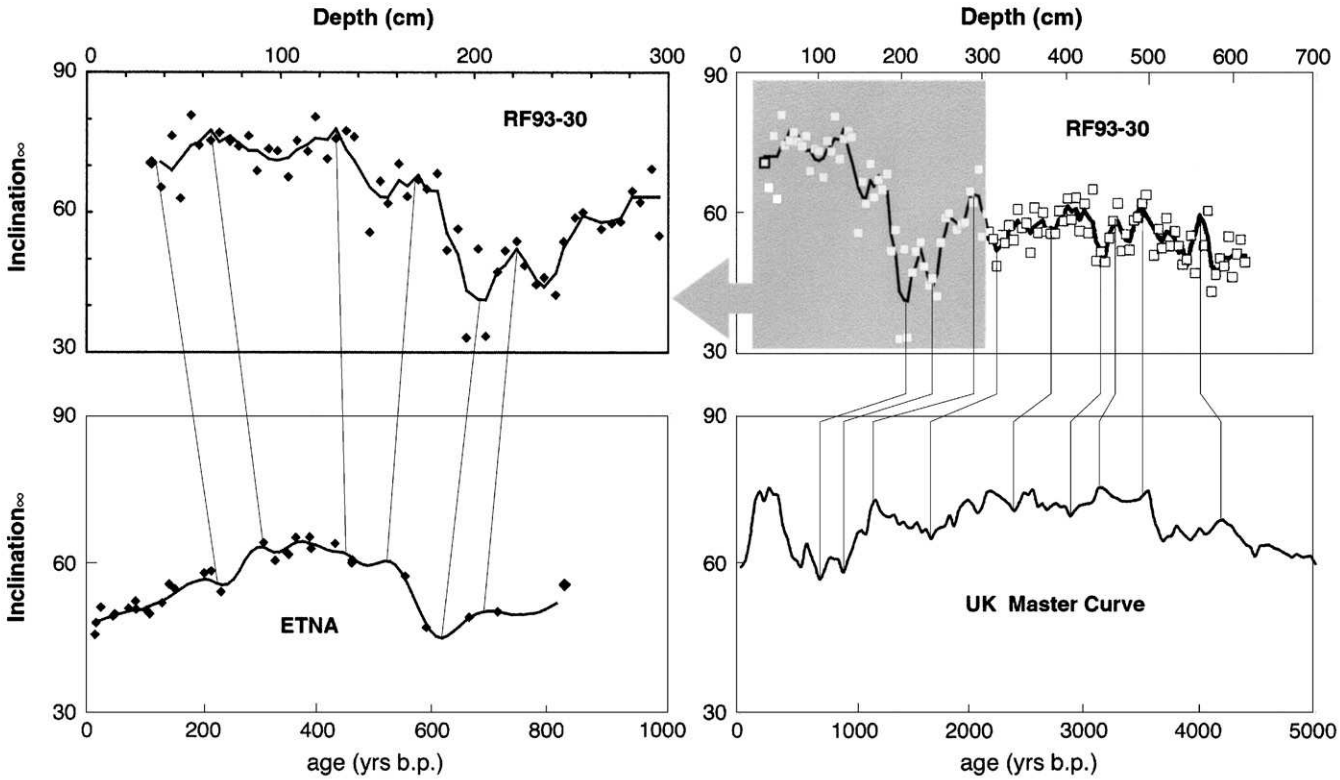


Fig. 10. Lines of proposed correlation linking the inclination record in RF 93-30 (Fig. 6) with the dated record from Mt Etna in the left hand graphs (Shaw and Rolph, 1986) and with the UK Master Curve in the right hand graphs (Turner and Thompson, 1981).

On the basis of the changes in the benthic foraminifera assemblage the core was divided into the following intervals.

Zone 1 (620–590 cm): the assemblage is mainly composed of *Brizalina spathulata* (up to 20%), *Uvigerina peregrina* and *Uvigerina mediterranea*, *B. marginata* m. aculeata. *Elphidium decipiens*, *Globocassidulina subglobosa* (14%), *Epistominella vitrea* (up to 10%) are also present. *Hyalinea balthica* is also present but with low percentages (5%).

Zone 2a (590–540 cm): *B. spathulata* shows high percentages (30%) while *Uvigerina* spp almost disappears. *Cassidulina laevigata carinata* increases and *B. marginata* morph aculeata is present (20%).

Zone 2b (540–390 cm): at the base of this interval *C. laevigata carinata* peaks; after that it displays a decreasing trend up to 270 cm, then its frequency remains low (<10%) and constant up to the top of the core. *B. spathulata* decreases sharply at the base of this interval. It is present throughout the core with values remaining lower than 10% save in the uppermost sample where they reach 20%. *Valvulineria complanata* shows high percentages between 480 and 400 cm.

Zone 2c (390–220 cm): *V. complanata* decreases displaying values lower than 10% throughout this interval while *E. decipiens* shows a relative increase.

Zone 2d (220–10 cm): *B. marginata* m. marginata shows an abrupt increase at 210 cm reaching values up to 15%. *V. complanata* displays several fluctuations (up to 40%).

Zone 2e (10–0 cm): abrupt increase of *B. marginata* m. marginata together with *B. spathulata* at the expense of *V. complanata*, *C. laevigata carinata* and *E. decipiens*. Also *E. vitrea* shows an increase, reaching 11%.

### *4.8. Alkenones (Fig. 9)*

$U^{k'}_{37}$ data were converted to temperature ($T$) using the relationship described by Müller et al. (1998).

$$U^{k'}_{37} = 0.033T + 0.044. \quad (2)$$

The $T$ data for RF93-30 show significant variation with sediment depth and time (Fig. 8), with a maximum between 13.8°C and 19.6°C. Oscillation in $T$ between 7000 and 6000 yr BP is followed by gradual warming then cooling to 3500 BP, after which there is a remarkable increase in $U^{k'}_{37}$-derived $T$ from ~13.8°C to ~19.6°C by 3000 yr BP and reversion to ~14°C by 2000 yr BP. More recently, at ~700 yr BP, $U^{k'}_{37}$-derived $T$ cooled rapidly from ~16°C to 13.8°C and has then gradually increased towards the top of the core (to ~18.5°C), before a reversal in the youngest intervals analysed (to ~17.5°C).

## 5. Chronology of sedimentation

All available lines of evidence have been considered in constructing a chronology of sedimentation for the core (Table 3). From 251 cm upwards, the main basis for the chronology is the strong correlation between the magnetic inclination trace (Fig. 10) and that for historically dated Etna lavas (Rolph and Shaw, 1986). Between 251 and 444 cm, the chronology largely relies on a correlation between the magnetic inclination record and the UK Master Curve (Fig. 10), (Turner and Thompson, 1981). In these parts of the core, the palaeomagnetic chronology proposed is significantly younger than that suggested by standard reservoir-corrected $^{14}$C dates based on benthic forams. The chronology is however consistent with the date at which *Zea* (maize) pollen is first encountered, the Roman introduction of *Juglans*, pollen of which is first encountered at 350 cm and the dates below 480 cm derived from pollen correlations with other $^{14}$C dated cores where planktonic forams were available for dating, as well as with the age of the Avellino tephra at 527 cm. Despite failure to identify shards of volcanic ash from sediments containing these upper SIRM spikes, the palaeomagnetic chronology proposed dates those at 116 and 294 cm very close to the ages of dated historical eruptions of Mt Somma (AD 1644) and Vesuvius (AD781) respectively—source ascriptions that are consistent with the similarity in the magnetic 'signatures' for the major SIRM spikes (Fig. 5). The age ascriptions based on the Etna correlation are probably accurate to a few decades at worst; those based on a correlation with Windermere (using a time-lag of 70 yr) are likely to be more approximate.

Below the Avellino tephra, the two planktonic foram-based $^{14}$C dates at 527 and 599 cm have been accepted. They fall in the same *zone* of planktonic foraminifera identified and dated in other cores in the Adriatic region (Asioli, 1996; Trincardi et al., 1996; Correggiari et al., 2000); these cores show ages that are consistent with those provided here. The top of the G. *inflata* zone (590 cm) is dated to 5.5 cal. ky BP and is assumed to coincide with the mfs on seismic profiles (Trincardi et al., 1996). The Avellino tephra (3.6 cal. ky BP) is in fact about 70 cm above the top of the G. *inflata* zone indicating an interval of condensed deposition (70 cm/1900 yr with an average sediment accumulation rate of 0.36 mm/yr) compared with 144 cm/kyr from 520 cm to the top of the core.

The composite chronology derived from these several lines of evidence (Fig. 11) has been used in Fig. 13 both as a timescale for representing the data and as a basis for calculating net depositional fluxes. The apparently unreliable benthic foram based $^{14}$C dates in the upper part of the core may be related to the changes in species composition (Fig. 8) and inferred stress-levels (see below) recorded in the assemblages present.

Table 3
Control points for the age-depth model for Core RF 93-30 (see Fig. 11)

| Core depth (cm) | Control point (yr BP) | Calendar age (yr) | Source | Note |
|---|---|---|---|---|
| 30 | 125 | 1865 AD | Paleomag (Etna) | |
| 69 | 210 | 1780 | Paleomag (Etna) | |
| 117[a] | 301[a] | 1689[a] | Paleomag (Etna) | |
| *129* | *640* | *1350* | *cal.* $^{14}$*C* | *Rejected* |
| 209 | 582 | 1408 | Paleomag (Etna) | |
| *219* | *1200* | *790* | *cal.* $^{14}$*C* | *Rejected* |
| 251 | 821 | 1169 | Paleomag (Etna) | |
| 289 | 1180 | 810 | Paleomag (Windermere) | |
| 317 | 1580 | 410 | Paleomag (Windermere) | |
| 355 | 2040 | 50 BC | Paleomag (Windermere) | |
| *365* | *2690* | *700* | *cal.* $^{14}$*C* | *Rejected* |
| 380 | 2320 | 330 | Paleomag (Windermere) | |
| 444 | 2800 | 810 | Paleomag (Windermere) | |
| 485 | 3100 | 1110 | Pollen (Avena/Triticum) | |
| 527 | 3660 | 1670 | cal. $^{14}$C and tephra SV | |
| 599 | 6170 | 4180 | cal. $^{14}$C | |

[a] Note that this age is consistent with the first occurrence of pollen of *Zea mays* (maize) at 132 cm.

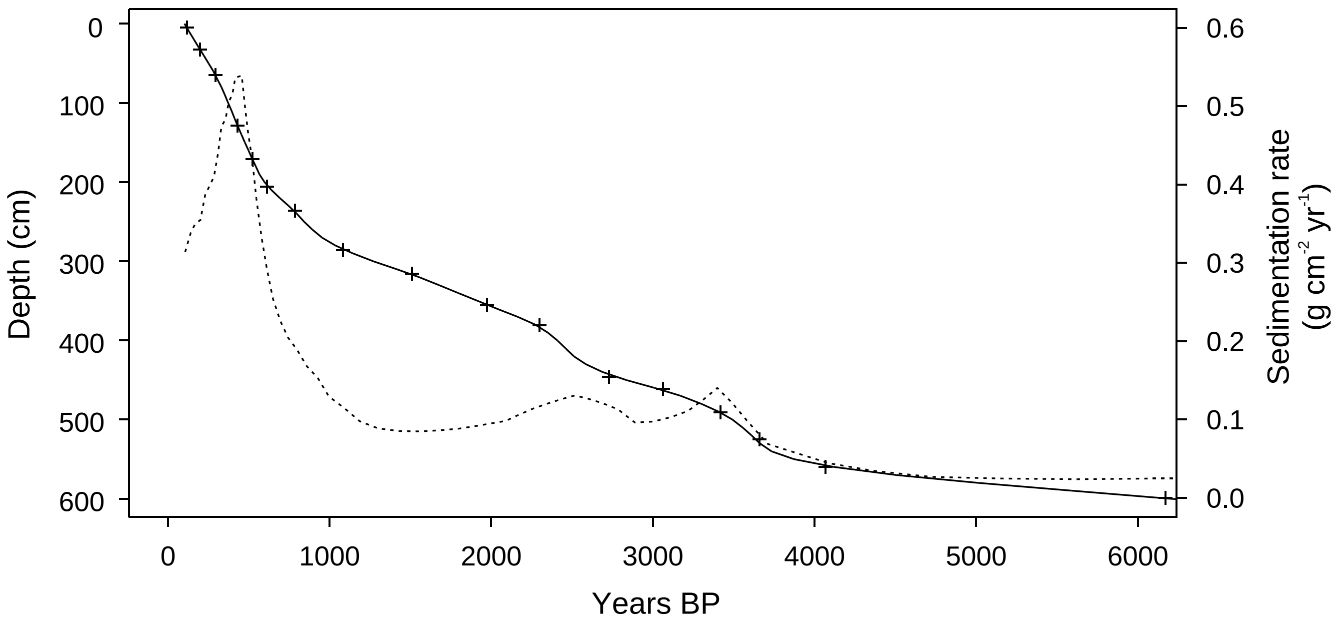


Fig. 11. The age/depth curve, shown as a solid line, is derived from a smoothing spline function through the dated points given in Table 3. The dry mass accumulation rate is shown as a pecked line.

## 6. Discussion

### 6.1. Terrestrial vegetation change and human impact

Interpretation of the pollen analytical data from the core can only be in very broad regional terms, for there is no clear evidence to indicate the balance of contributions from airborne or waterborne pathways, nor, within the latter, the balance between local river sources and the more remote major rivers such as the Adige and Po to the north. Evidence from estuarine (Brush et al., 1982) and large reservoir (Clark, 1986) systems suggests that in such environments, waterborne pathways are likely to have been significant and that pollen behaves much like the silt grade in the sediments. This implies a potentially large and diverse pollen source area including both the lower Po valley and the eastern flanks of the north and central Appenines. The inference of dominantly sediment-associated supply pathways is reinforced by the fact that pollen concentrations in the core are not diluted during periods of increased sedimentation; in some cases they reach peak values (Lowe et al., 1996).

Although there are traces of human impact on the predominantly forested landscapes within the pollen source area prior to 3600 BP, the first dramatic change in land cover coincides closely with the age of the Avellino Tephra and leads to a maximum extent of deforested land around 3000 BP. The record thus parallels that from the crater lakes Albano and Nemi (Lowe et al., 1996) close to Rome as well as the pollen, charcoal, sedimentological and archaeological results summarized in Ramrath et al. (2000). It suggests that Late Bronze Age forest clearance had a major, widespread impact on the landscape in northern and central Italy. There are clear signs of increased cereal and olive cultivation; deciduous tree representation declines steeply and the overall non-tree pollen percentage contribution in the pollen diagram doubles. Subsequently, there is evidence for a slow recovery of deciduous forest cover from ca 3000 to 1500 BP, but with signs of cultivation throughout the period.

The evidence in all the pollen sequences quoted includes strong signs of human activity, including cereal cultivation, and it is difficult to avoid the conclusion that these activities have had a major impact on both vegetation and surface processes. There remains however the real possibility that the record is also significantly influenced by climate change, especially a trend to dessication. This is the favoured explanation of Jalut et al. (2000) working further west in the Mediterranean basin. As with the later episode of strong human impact noted below, the observed synchroneity between the changes and variations in sea-surface temperature would tend to support this argument (see below).

The next decline in forest cover begins around 1100 BP, then steepens between 700 BP (AD 1250) and 600 BP. From this time on, through the Medieval and most recent period recorded, signs of cultivation and reduced forest cover persist. It is at the beginning of this period that the ratio of *Quercus ilex* to *Juniperus* pollen is reversed in favour of the latter, suggesting that this may have been a period during which there was a tendency for the Mediterranean evergreen woodland to degrade to scrub. Once more, there is a strong parallel with the results from Lago Mezzano in C Italy (Ramrath et al., 2000), as well as with those of Atherden and Hall (1999) from Crete.

One notable feature common to both this marine sequence and the lacustrine ones noted from C Italy is absence of any strong indication of human impact on vegetation during the Roman period.

### 6.2. Land cover change and sediment flux

The two main episodes of forest clearance and extension of cultivation, between 3600 and 3000 BP and around 700 to 600 BP are marked by increases in total sediment flux to the site. The rates of net sediment flux from early medieval times onwards exceed the pre-Late Bronze Age rates by a factor of 6–7. The later parts of each period of minimum forest cover are also associated with low values for both the percentage contribution (never in excess of 0.6%) and the flux of TOC. These results are therefore consistent with the interpretation of the sediments within the HST which Core RF 93-30 represents, as a plume of terrigenous sediment and suggest a strong link between land cover, surface processes and near-shore marine sedimentation. Where there is a link between low forest pollen percentages and generally reduced TOC values, it would suggest that during the later stages of deforestation, the sediment supply comprised predominantly mineral soils; the precise phasing of changes is considered in the next section.

The period of modestly increased mass sedimentation centred around 2400 BP is not associated with changes in pollen indicative of deforestation, nor is there a clear response in the benthic foram record. This period is believed to have been one of increased rural settlement during Samnite and Roman times, with strong evidence for accelerated soil erosion in the nearby Biferno valley region (Barker, 1995). It is therefore possible that the sedimentation records an anthropogenic impact not clearly distinguishable from the pollen record.

### 6.3. Magnetic evidence for sediment sources

We propose an interpretation of the magnetic properties of the sediments in terms of four components.

1. Both the confirmed tephra layer at 525–530 cm and the later, similarly discrete SIRM spikes (Fig. 5) are marked by higher magnetic concentrations and SIRM/$\kappa$ quotients as well as reduced values for HIRM, $\kappa_{ARM}/\kappa_{LF}$ and ARM/SIRM. A more consistently crystalline assemblage dominated by relatively coarser grained magnetites is indicated. Absence of additional non-magnetic evidence to support the volcanic origin of the upper magnetic 'spikes' is difficult to explain. In magnetic studies of beach and near shore sands elsewhere (e.g. Lees and Pethick, 1995) similar magnetic assemblages have been found in areas of heavy mineral enrichment and this is one possible alternative interpretation.
2. It is apparent from the TEM analyses of sediments from the lower part of the core that the fine-grained magnetite that dominates the magnetic record between the tephra layers is rich in bacterial magnetosomes. This is in good agreement with previous interpretations of the high ARM/SIRM quotient values (consistently in excess of $2 \times 10^{-3}$ when the ARM values are normalized to the DC bias field) in the Holocene sediments in this and other cores from the south and central Adriatic (Oldfield, 1994; Oldfield et al., 1995; Oldfield and Frignani, 1995; Rolph et al., 1996). Oldfield and Frignani (1995) provide supporting evidence for this interpretation by plotting the changes in magnetic properties in a suite of shallow dated cores taken at increasing distances from the Po Delta southwards. Whereas the magnetic concentration indicators reflecting terrigenous flux show values declining with distance from the Po delta, $\chi_{ARM}$/SIRM values increase steeply over the first 25–30 km, then more gently, towards the kinds of values found in the mid-Adriatic (Fig. 12). This is in keeping with the view that high ARM and $\chi_{ARM}$/SIRM values are indicative of an autochthonous biogenic source of magnetite.
3. The third component is most clearly characterized by the percentage contribution to the total SIRM of magnetically 'hard' remanence carrying minerals in the core (Hard IRM%). This anti-ferromagnetic component, representing haematite and goethite, makes a relatively low contribution to the tephra horizons and between these, varies largely in antiphase with the values for ARM and the quotients that use ARM or $\kappa_{ARM}$ as the numerator. Its variations almost perfectly parallel the non-tree pollen percentages and indicators of cultivation and human disturbance, just as ARM varies in parallel with tree pollen percentages. We therefore interpret this 'hard remanence' component as indicative of eroded terrigenous minerogenic material.
4. A fourth component responsible for the changes in $\kappa_{ARM}/\kappa_{LF}$ that parallel variations in ARM and are opposed to the changes in 'hard' IRM% is more difficult to identify unambiguously. Declines in this quotient may represent increased paramagnetic contributions as well as either coarsening or fining of the magnetic grain size, depending on whether the ferrimagnetic grain sizes present are dominantly pseudo-single domain (PSD) and multi-domain (MD) (King et al., 1982) or stable single domain (SD) and finer superparamagnetic (SP) grains (Oldfield, 1994). The consistently high values for $\kappa_{ARM}$/SIRM and the values for $\chi_{fd}$% in excess of

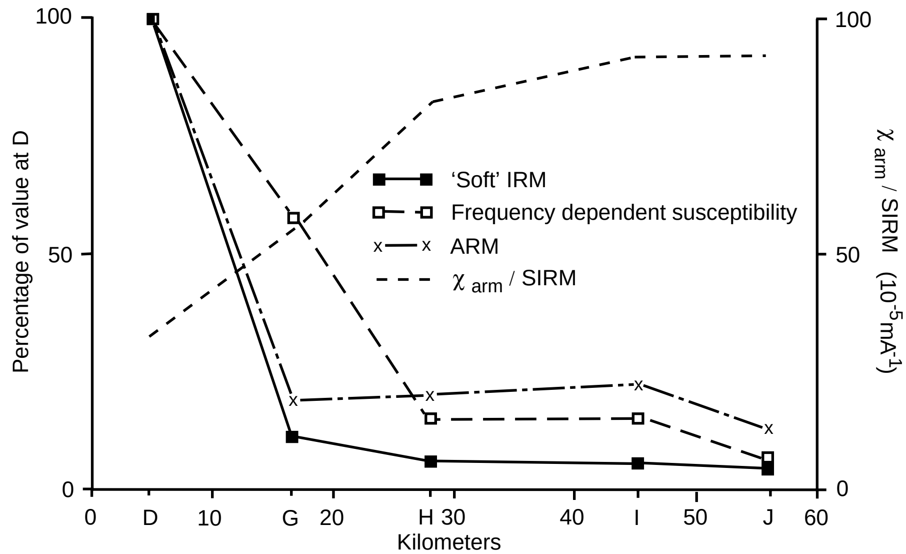


Fig. 12. Changes in the flux of magnetic minerals and in the values of $\chi_{ARM}$/SIRM in a series of recent dated sediment cores at different distances from the delta of the river Po (Oldfield and Frignani, 1995). 'Soft' IRM ($IRM_{20mT}$), Frequency dependent susceptibility ($\chi$fd) and ARM all represent components of the magnetic mineral flux to the sediments. The flux values are expressed as percentages of the value calculated for core D, the nearest to the delta. All the values decline steeply with distance, indicating that there is a strong terrigenous contribution to each. ARM declines least steeply and the values for the quotient $\chi_{ARM}$/SIRM rise with distance from the delta, towards the values typical of Holocene sediments in the open Adriatic (Oldfield et al., 1995, and this paper). This supports the view that the ARM values and the quotients derived from these are influenced by a non-terrigenous contribution.

4% throughout confirm that the latter interpretation is the more likely. We therefore interpret the periods of lowered $\kappa_{ARM}/\kappa_{LF}$, corresponding with increased Hard IRM as indicating increases in the paramagnetic and/or superparamagnetic component in the sediments. The underlying changes in $\chi_{fd}$% noted above also support this interpretation. In earlier cores from the central Adriatic (Oldfield et al., 1995), the late Holocene is marked by an increase in $\chi_{fd}$% values indicative of increased soil erosion (Dearing et al., 1996). At the same time an increase in paramagnetic iron and/or SP grains, inferred from the reduction in the $\kappa_{ARM}/\kappa_{LF}$ values is also consistent with a record of increased soil erosion contributing to the sediments in the core.

If we consider these inferences more closely alongside the pollen and TOC data, a clearer distinction emerges between the early and later stages of the two main episodes of deforestation. During the first stages of Late Bronze Age (3.6 cal. ka BP) forest clearance the pollen and magnetic properties respond in phase, but TOC% values increase before falling to minimum values. Similarly, during the earlier stages of the medieval forest clearance, TOC% values remain relatively high, only reaching minima in sediments that just predate the increase near the sediment-water interface that may be either a reflection of further human impacts or a diagenetic gradient. The likely interpretation of these sequences is that the early forest-clearance, higher values in TOC% represent input of terrigenous material as stable organic residues from surface soils, whereas during the later stages of deforestation and human impact, eroded material is less rich in organic matter and more likely to be derived from deeper in the regolith.

### 6.4. The benthic foram record: anthropogenic impacts

The record of changes in the benthic formaniferal assemblages is interpreted in light of the model proposed by Van der Zwaan and Jorissen (1991) which seeks to explain the seasonal changes in microhabitat selection by benthic foraminifera living in the Adriatic Sea clay belt. It is based on two assumptions: (1) the oxygen level in the sediment column is a limiting factors controlling the presence of infaunal life and (2) several taxa are exclusively epifaunal while others are infaunal during periods of well oxygenated bottom waters (e.g. winter) and shift to epifaunal position during periods of low oxygen concentrations in the sediments (e.g. summer and autumn). Although the present study was carried out on the >63 mm fraction and that of Van der Zwaan and Jorissen (1991) based their model on >150 μm fraction, all the evidence available (such as near-absence of *E. vitrea*, absence of *Hopkinsina* and *Stainforthia*, all species that may dominate the fraction 63–150 mm in the Van der Zwaan and Jorissen's model) suggests that their model is applicable to the present study.

In an additional study carried out in the Northern Adriatic on the contemporary living benthic foraminifera, Barmawidjaja et al. (1992) considered the species

*Brizalina dilatata*, *B. spathulata*, *B. marginata*, *E. vitrea* and *Hopkinsina* as potentially infaunal taxa. This group of species is believed to invade the sediment and reach the maximal living depth in February, then to shift their microhabitat towards the sediment water interface when the oxygen values decrease during dysoxic period in late summer. Barmawidjaja et al. (1992) consider these (apparently) very mobile species the least sensitive to hypoxia and typical of the low oxygen environment and suggest that they may have the ability to track oxygen gradients. Consequently, the sum of the species belonging to this group and present in core RF93-30 (see Fig. 8b) (*B. dilatata* + *B. spathulata* + *B. marginata* + *E. vitrea*) may be regarded as an indicator of the frequency of dysoxic episodes.

One of the major faunal changes present in core RF93-30 is located between interval 1 and 2a (590 cm, between 6000 and 5500 BP). *V. complanata*, *B. marginata* and *Nonionella turgida* occur throughout interval 1 from this point onwards. These three species are typical of the modern clay belt, a food saturated environment according to Barmawidjaja et al. (1992), and they are also considered opportunistic taxa tolerant of reduced oxygen conditions and preferring increased nutrient levels (van der Zwaan and Jorissen, 1991). Although several species as *B. marginata* m. aculeata and *B. spathulata* were already present at zone 1, indicating the presence of low oxygen values in the bottom water at least seasonally, it seems that bottom conditions comparable to those prevailing within the modern clay belt occurred from the base of zone 2 onwards.

Interval 2a is characterized by the presence of potentially infaunal taxa, suggesting that dysoxic periods occurred. Cores collected in the Middle Adriatic Depression (e.g. CM92-43, RF93-77, Pal94-77, Pal94-8, Pal94-9) (Asioli, 1996; Trincardi et al., 1996) at greater depth show that between 6 and 8 ka BP an important benthic foraminifera change took place. *B. spathulata* increases in frequency while species such as *H. balthica* and *Uvigerina* spp, previously quite common, display an abrupt decrease. Although several differences are present in the benthic assemblages between core RF93-30 and the deeper cores within this interval, such as the presence of *B. marginata* m. aliniti and *E. decipiens* in core RF93-30 replaced by *Cibicidoides pachyderma* and *Uvigerina* spp in the deeper cores, overall the evidence indicates that in the area of core RF93-30 and the deeper areas where the other cores were collected the bottom conditions were somewhat similar.

A major change occurs at the base of interval 2b (540 cm = ca 4000 BP) which, in terms of the interpretative model adopted, can best be interpreted as an increase in the influence of fluvial input, very low at the base (high frequency of *C. laevigata carinata* that occupies the area minimally affected by river runoff) and stronger upward between 470 and 400 cm (between ca 3000 and 2400 BP) where *V. complanata* peaks and the potentially infaunal taxa show a weak increase. This is the Late Bronze Age period of maximum deforestation and inferred soil erosion. Van der Zwaan and Jorissen (1991) stress the high impact of increased terrestrially derived nutrient, organic matter and sediment input for the types of benthic communities recorded here. We therefore suggest that the parallels between the pollen, sedimentation rate, magnetic and benthic foram records over this period confirms that human activity on land already had a significant effect on near-shore benthic fauna as a result of the resulting increases in fluvially derived material.

The interval 2c (390–220 cm = ~2400–640 BP) shows the lowest percentages of the potentially infaunal taxa. Together with the decrease of *V. complanata* this is likely to indicate a reduced fluvial runoff. It is noteworthy that the planktonic species *G. sacculifer*, although present only in low numbers, peaks in the lower part of the interval 2b and within the whole of 2c. *G. sacculifer* is a symbiont bearing species that dwells in oligotrophic mixed layers (Hemleben et al., 1989). According to the interpretation based on benthic foraminifera, the two intervals where this species peaks seem to correspond to periods of reduced terrestrial/fluvial influence compared with the intervening later part of 2b, as well as lower nutrient input and, consequently, lower water turbidity. This accords well with the environmental requirements of *G. sacculifer*. In terms of the record of deforestation and erosion outlined above, this is a period of forest recovery and reduced terrigenous input. The record detected by these foraminifera is not local: in other cores collected in the clay belt at water depth ca 50m and located 300 km northward of core RF 93-30, the same fluctuations of the key species have been found (Roveri et al., 1998).

In the interval 2d the fluvial influence seems to increase again. The potentially infaunal taxa increases, *C. laevigata carinata* shows the lowest values while *B. marginata* m. denudata, the more oxygen tolerant species, is present, although with low percentages. This situation probably indicates more stressed bottom conditions, although the most severe conditions depicted by Van der Zwaan and Jorissen (1991), such as the dominance of *B. marginata* m. denudata or the absence of benthic forams, are not recorded in RF93-30. It is once more noteworthy that the period of inferred fluvial influence and increased stress corresponds with a major episode of deforestation and erosion.

Finally, the top of the core, representing some period within the last two centuries is characterized by an abrupt increase in the potentially infaunal taxa, mainly caused by the increase of *B. marginata* m. marginata and *B. spathulata*. This is tentatively interpreted as a response to more frequent episodes of low oxygenation of the bottom water, increasing the relative importance of taxa more able to migrate within the sediment column.

Overall, one of the most notable features of the benthic foram record is the consistent link between evidence for deforestation, accelerated sedimentation and erosive input on the one hand and the responses to consequent environmental stresses in the benthic record.

### 6.5. Calibration of $U_{37}^{k'}$

The relationship between $U_{37}^{k'}$ and $T$ described by Müller et al. (1998) was determined by examination of sediment core tops from the Atlantic, Pacific and Indian Oceans between 60°N and 60°S. Eq. (2) is similar to that originally derived by Prahl and Wakeham (1987) and holds well even at relatively high temperatures (25–29°C; Pelejero and Grimalt, 1997; Sonzogni et al., 1997), but less so at very low temperatures ($<5$°C; e.g. Sikes et al., 1997). Recently, Ternois et al. (1997) carried out a seasonal study of particulate organic material in the Mediterranean and after calibration with CTD data, derived a rather different relationship between $T$ and $U_{37}^{k'}$:

$$U_{37}^{k'} = 0.041T - 0.21. \quad (3)$$

This equation consistently gives higher $T$ values, by about 3–4°C than that derived by Müller et al. (1998), but the Ternois et al. (1997) relationship appears to be valid when considering water column particulate matter samples (Cacho et al., 1999). On the other hand, examination of core top samples from the Mediterranean, which are by definition time averaged, show that $T$ values determined according to Ternois et al. (1997) are consistently much higher than the mean annual SST, or average temperature for the mixed layer (Cacho et al., 1999). One possible explanation for this discrepancy is that the time series studied by Ternois et al. (1997) was through spring and summer, whereas the period of dominance of Haptophyte (coccolith) species in Mediterranean waters is skewed to the late summer and early autumn (Cacho et al., 1999). A similar situation is apparent for the Adriatic where coccoliths are relatively minor components of the phytoplankton, but dominate in the autumn and winter (Misserochi et al., 1998; Mozeti et al., 1998). For these reasons the relationship described by Müller et al. (1998; Eq. (2)) is preferred for the RF93-30 core.

It is important to consider whether the relatively shallow water depth for the RF93-30 core and its proximity to the coast, may also have some influence on the $U_{37}^{k'}$ derived temperature, particularly with respect to the influence of the Po river outflow. At low salinities, high amounts of the tetraunsaturated $C_{37}$ alkenone are often present; these likely derive from fresh or brackish water species that become dominant at low salinities and certainly influence $U_{37}^{K}$ values (Conté et al., 1994; Ficken and Farrimond, 1995). However, analysis of the core samples by GCMS in electron impact mode, with collection of full mass spectra indicated that these compounds were absent in the RF93-30 samples. Thus it is unlikely that the species that dominate low salinity environments have contributed to the sedimentary record. It should be noted that even at times of elevated outflow of the Po, it is highly unlikely that the salinities of surface water in the Adriatic have decreased to less than 35.

Finally, it should be noted that the $U_{37}^{k'}$-derived $T$ reflects the mean water temperature of the euphotic zone during the period of maximum production by coccolithophores, which may not correspond to the annual mean surface water $T$. Furthermore, the $U_{37}^{k'}$-derived $T$ reflects the temperature of the zone of maximum production by the coccoliths, which may be as deep as 30 m in a stratified water column (Bentaleb et al., 1999). The derived temperatures also assume that there has not been any significant alteration in the ratio of diunsaturated to triunsaturated alkenones as a result of preferential diagenetic degradation of the $C_{37:3}$ compound.

### 6.6. $U_{37}^{k'}$-derived temperature record for RF93-30

The range of $U_{37}^{k'}$-derived temperatures (13.8–19.6°C) (Fig. 9) are consistent with those observed in deeper water Adriatic cores (Ariztegui et al., 1996) and are within the range reported for the Mediterranean Sea over the period of the last 16,000 yr (11.4–23.6°C; Emeis et al., 2000). Moreover, the most recent values are consistent with those summarized for the 20th century by Artegiani et al. (1997). The most significant changes observed in the RF93-30 core are between 3500 and 2000 yr BP, when temperature apparently increased rapidly over 500 yr from 13.8°C to 19.6°C, before cooling again by 2000 yr BP (Fig. 13). These changes correspond closely with palaeosalinity variations in Levantine Seawater (LSW), whose salinity decreased by 2–3 psu between 3500 and 3000 yr BP, before increasing by 4–5 psu by 2000 yr BP (Emeis et al., 2000). The salinity of LSW is an important variable when considering RF93-30, since it forms the intermediate water in the middle Adriatic sub-basin at the core location (e.g. Artegiani et al., 1997). Thus, at present, relatively fresh surface waters (salinity of $\sim$37.7–38.3) overlie North Adriatic Deep Water (NadDW) in the summer ($\sim$38.5); the latter is modified by inflow of Mid-Levantine Intermediate Water (MLIW) which intrudes into the region between the spring and autumn to form Mid-Adriatic Deep Water (MadDW). An inflow of fresher surface waters would be expected to lead to an intensification of salinity stratification; on the other hand, a reduction in the salinity of the MLIW (as occurred between 3500 and

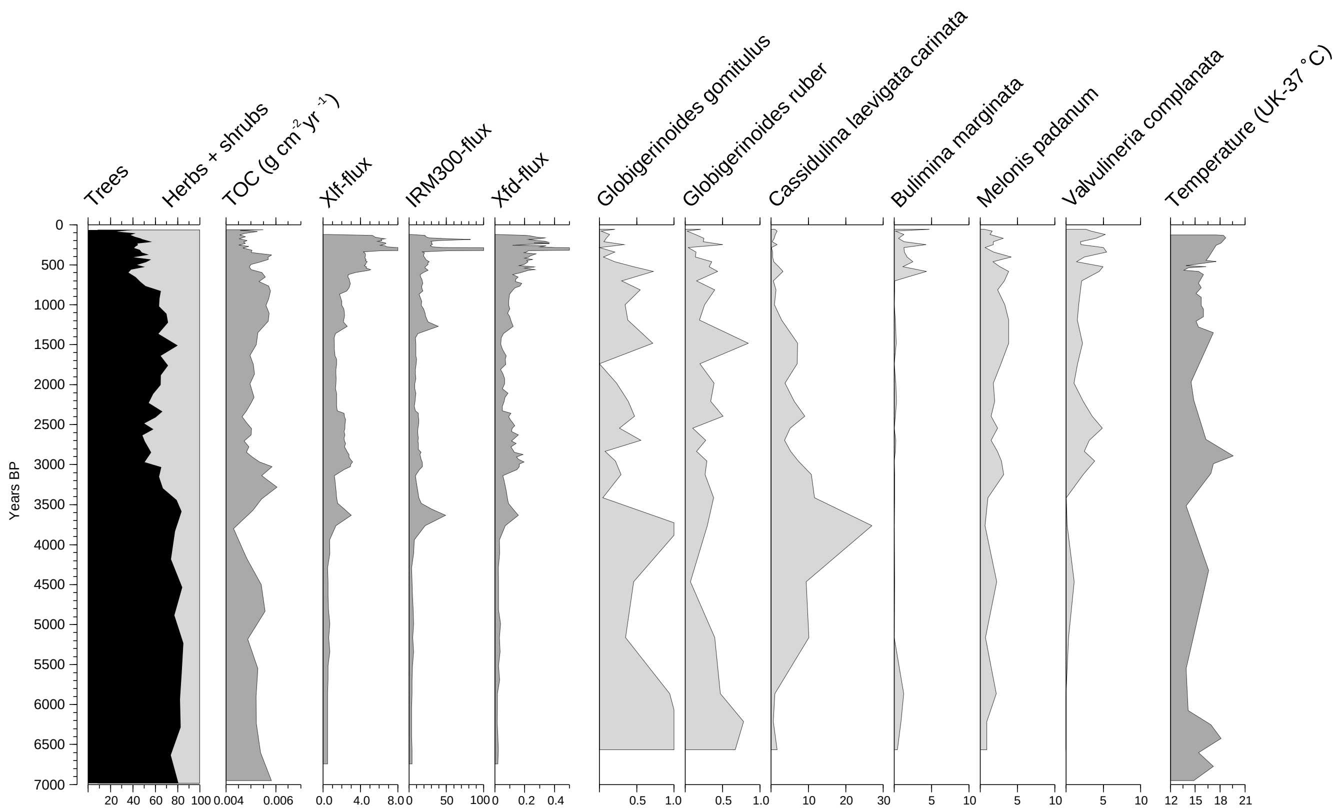


Fig. 13. Selected proxy records plotted against the timescale derived from the age/depth model (Fig. 12a and Table 3).

3000 yr BP; Emeis et al., 2000), would be expected to reduce stratification and potentially deepen the halocline (more mixing). Such effects would be likely to influence $U^{k'}_{37}$–derived $T$, since a deeper halocline and more mixing between NadDW and MLIW would lead to a deeper thermocline and a higher mean $T$ over the dominant zone of production of the alkenones by coccolithophores (10–40 m; Cacho et al., 1999). Over the period from 3500 to 3000 yr BP therefore, the apparent change in sea-surface temperature as determined by $U^{k'}_{37}$ probably reflects increased mixing of the water column. Between 3000 and 2000 yr BP, the salinity of MLIW again increased, enhancing stratification and leading to the shoaling of the thermocline, thus reversing the apparent warming.

Shorter-term fluctuations, e.g. between 7000 and 6000 and the rapid cooling at ~600 yr BP could also be attributed to changes in stratification. Although the salinity of the MLIW probably did not vary dramatically over that period (Emeis et al., 2000), enhanced outflow from the River Po, which coincides with land clearance and enhanced sedimentation rates, could have lead to freshening of surface waters and increased stratification, thus leading to shoaling of the thermocline during periods of apparently cool $U^{k'}_{37}$ temperature. Conversely, the warmer $U^{k'}_{37}$ temperature observed by 500 yr BP probably reflects decreased river outflow and evaporation, which would have resulted in deepening of the thermocline through enhanced mixing of more saline surface waters with the MadDW. The degree of stratification of the Mid-Adriatic Basin and the prevailing atmospheric conditions over the past 700 yr are likely to have been closely linked.

## 7. Conclusions

Fig. 13 presents a summary of the key results plotted against the chronology outlined in Table 3 and Fig. 11. The present interpretation of the results of a multi-proxy analysis of Adriatic Core RF 93-30 points to the following conclusions:

1. Vegetation change reflecting human activity dominates the pollen record, at least from 3600 BP to the present day, though the role of climate change as a trigger to cultural change and/or as an amplifier of human impact cannot be excluded. The most striking episodes of deforestation and expanding human impact begin around 3600 BP (1650 BC), (Late Bronze Age), and 700 BP (AD 1250), (Medieval), and each leads to an acceleration in mass sedimentation and an increase in the proportion of terrigenous material, reflecting the response of surface processes

to widespread forest clearance and cultivation. A more modest increase in sedimentation around 2400 BP (450 BC) is not paralleled by any strong changes in pollen percentages.

2. Human activity, documented through the pollen record and leading to accelerated erosion during periods of deforestation and extended agriculture, drives the main changes in magnetic properties in all parts of the core not affected by tephra deposition. Erosive input, characterized by magnetic properties that can be linked to allogenic, terrigenous, rather than autochthonous, biogenic sources, perfectly tracks the pollen analytical evidence for land disturbance, forest clearance and cultivation.
3. Sedimentation rates roughly quadrupled between 1100 and 700 yr ago in response to land use changes and associated increases in terrigenous sediment yield. Pollen analytical evidence suggests that this period was one during which the decline of Mediterranean evergreen forest elements and the spread of scrub vegetation took place, thus suggesting that this was perhaps the period of most severe land degradation in the extensive pollen and sediment source areas for this core.
4. Both major episodes of human activity and consequent erosion, but especially the later one, gave rise to changes in the assemblage of benthic foraminiferal morphotypes indicative of increased levels of stress within the marine ecosystem arising from accelerating sedimentation and reduced oxygen availability.
5. With regard to the above conclusions it is important to realise that the record of changing sedimentation rates reconstructed for a single core cannot yet be taken as representative of the large scale sedimentation rates for the whole area of recent fine sediment deposition along the western flank of the Adriatic. On the other hand the evidence for links between human activity and sediment yield is quite robust; moreover knowledge of the stratigraphy of late Holocene sedimentation in the Adriatic, coupled with the readily identifiable and precisely dated tephra layers provides a chronostratigraphic framework within which confident quantification will be possible.
6. The present approach, combining a range of proxy indicators, including $U_{37}^{k'}$ promises to help to disentangle human and climate effects during the Late Holocene, provided it proves possible to infer climatic changes from the near-shore and relatively shallow-water alkenone record with more confidence than is possible at present.

## Acknowledgements

The results presented here form part of PALICLAS (Palaeo-environmental Analysis of Italian Crater Lake and Adriatic Sediments), an international project largely funded through EU Contract no. EV 5V-CT 93-0267. We are grateful to Prof J.R. Maxwell, FRS for his gift of alkenone standards and to Gareth Harriman for chemical ionization GCMS analyses. We would also like to thank Valerie Hall of the Paleoecology Laboratory, Queens University, Belfast who kindly examined material from the inferred tephra layers in the upper part of the core. Two anonymous referees made many suggestions that have helped to improve the paper.

## Note added in proof

In Section 5 of the paper we refer to the tephra at 527 cm as the Avellino Tephra, in view of its age and the position of the core directly in the path of the pumice fall deposits from that major eruption. Calanchi et al. (1998) cast doubt on this ascription on geochemical grounds and assign it an 'unclassified' status. One possibility, yet to be evaluated, is that it refers to the Astroni tephra, recently identified by Siani et al. (2001) in a core collected from the southern Adriatic. The age range for that tephra (4291–4146 cal. yr BP) is, however, somewhat old relative to the $^{14}C$ and Palaeomagnetic Secular Variation dates upon which the chronology for that part of the core is based.

## References

Alvisi, F., Frignani, M., 1996. $^{210}Pb$-derived sediment accumulation rates for the central Adriatic Sea and crater lakes Albano and Nemi (central Italy). In: Guilizzoni, P., Oldfield, F. (Eds.), Palaeoenvironmental Analysis of Italian Crater lake and Adriatic Sediments (PALICLAS). Memorie del'Istituto Italiano di Idrobiologia 55, pp. 303–320.

Ariztegui, D., Chondrogianni, C., Wolff, G., Asioli, A., Teranes, J., Bernasconi, S., McKenzie, J.A., 1996. Paleotemperature and paleosalinity history of the Meso Adriatic Depression (MAD) during the Late Quaternary: a stable isotopes and alkenones study. In: Oldfield, F., Guilizzoni, P. (Eds.), Palaeoenvironmental Analysis of Italian Crater Lake and Adriatic Sediments. Memorie dell'Istituto Italiano di Idrobiologia 55, 219–230.

Artegiani, A., Bregant, D., Paschini, E., Pinardi, N., Raicich, F., Russo, A., 1997. The Adriatic Sea general circulation. Part I: air-sea interactions and water mass structure. Journal of Physical Oceanography 27, 1492–1514.

Asioli, A., 1996. High resolution Foraminifera biostratigraphy in the Central Adriatic basin during the Last Deglaciation: a contribution to the PALICLAS project. In: Guilizzoni, P., Oldfield, F. (Eds.), Palaeoenvironmental Analysis of Italian Crater lake and Adriatic Sediments (PALICLAS). Memorie del'Istituto Italiano di Idrobiologia 55, pp. 197–218.

Asioli, A., Trincardi, F., Lowe, J.J., Oldfield, F., 1999. Short-term climate changes from the Central Adriatic basin during the Late-Glacial: comparison with other Mediterranean records and GRIP event stratigraphy. Journal of Quaternary Science 14, 373–381.

Asioli, A., Trincardi, F., Lowe, J.J., Ariztegui, D., Langone, L., Oldfield, F., 2001. Sub-millennial climatic oscillations in the Central Adriatic during the last deglaciation: paleoceanographic implications. Quaternary Science Reviews 20, 33–53.

Atherden, M.A., Hall, J.A., 1999. Human impact on vegetation in the White Mountains of Crete since AD 500. The Holocene 9, 183–193.

Barker, G., 1995. Land Use and Environmental Degradation in Biferno valley (Central Southrern Italy) from Prehistoric Times to the Present Day. L'Homme et la Degradation de l'Environment. XV$^e$ Rencontres Internationales d'Archaeologie d'Histoire d'Antibes. Editions APCDA, Juan-les-Pins.

Barmawidjaja, D.M., Jorissen, F.J., Puskaric, S., van der Zwaan, G.J., 1992. Microhabitat selection by benthic foraminifera in the Northern Adriatic Sea. Journal of Foraminiferal Research 22, 297–317.

Bartolini, C., Caputo, R., Pieri, M., 1996. Pliocene Quaternary sedimentation in the Northern Apennine Foredeep and related denudation. Geological Magazine 133, 244–273.

Bentaleb, I., Grimalt, J.O., Vidussi, F., Marty, J.-C., Martin, V., Denis, M., Hatté, C., Fontunge, M., 1999. The $C_{37}$ alkenone record of seawater temperature during seasonal thermocline stratification. Marine Chemistry 64, 301–313.

Brassell, S.C., Eglinton, G., Marlowe, I.T., Pflaumann, U., Sarnthein, M., 1986. Molecular stratigraphy: a new tool for climatic assessment. Nature 320, 129–133.

Brush, G.L., Martin, E.A., Dr Fries, R.S., Rice, C.A., 1982. Comparisons of $^{210}$Pb and pollen methods for determining rates of estuarine sediment accumulation. Quaternary Research 18, 196–217.

Cacho, I., Pelejero, C., Grimalt, J.O., Calafat, A., Canals, M., 1999. $C_{37}$ alkenone measurements of sea surface temperature in the Gulf of Lions (NW Mediterranean). Organic Geochemistry 30, 557–566.

Calanchi, N., Dinelli, E., Luchini, F., Mordenti, A., 1996. Chemostratigraphy of late Quaternary sediments from lake Albano and central Adriatic Sea cores. In: Guilizzoni, P., Oldfield, F. (Eds.), Palaeoenvironmental Analysis of Italian Crater Lake and Adriatic Sediments (PALICLAS). Memorie del'Istituto Italiano di Idrobiologia 55, pp. 247–264.

Calanchi, N., Cattaneo, A., Dinelli, E., Gasparotto, G., Lucchini, F., 1998. Tephra layers in late-Quaternary sediments of the central Adriatic Sea. Marine Geology 149, 191–209.

Clark, R.L., 1986. Pollen as a chronometer and sediment tracer, Burrinjuck reservoir, Australia. Hydrobiologia 143, 63–69.

Conte, M.H., Thompson, A., Eglinton, G., 1994. Primary production of lipid biomarker compounds by *Emiliania huxleyi*—results from an experimental mesocosm study in fjords of southwestern Norway. Sarsia 79, 319–331.

Correggiari, A., Roveri, M., Trincardi, F., 1996. Late-Pleistocene and Holocene evolution of the North Adriatic Sea. In: Late-Glacial and Early Holocene Climatic and Environmental Changes in Italy. Il Quaternario. Italian Journal of Quaternary Sciences 9(2), 697–704.

Correggiari, A., Trincardi, F., Langone, L., Roveri, M., 2001. Styles of failure in heavily sedimented highstand prodelta wedges on the Adriatic shelf. Journal of Sedimentary Research 71/2, 218–236.

Davies, S.M., Branch, N.P., Lowe, J.J., Turney, C.S.M., 2001. Towards a European tephrochronological framework for Termination 1 and the Early Holocene. Philosphical Transactions of the Royal Society of London, Series A 360, 767–802.

Dearing, J.A., Dann, R.J.L., Hay, K., Lees, J.A., Loveland, P.J., Maher, B.A., O'Grady, K., 1996a. Frequency-dependent susceptibility measurements of environmental materials. Geophysical Journal International 124, 228–240.

Emeis, K.-C., Struch, U., Schulz, H.-M., Rosenberg, R., Bernasconi, S., Erlenkeuser, H., Sakamoto, T., Martinez-Ruiz, F., 2000. Temperature and salinity variations of Mediterranean Sea surface waters over the last 16,000 years from records of planktonic stable oxygen isotopes and alkenone unsaturation ratios. Palaeogeography, Palaeoclimatology and Palaeoecology 158, 259–280.

Faganeli, J., Pezdic, J., Ogorelec, B., Misic, M., Najdek, M., 1994. The origin of sedimentary organic matter in the Adriatic. Continental Shelf Research 14, 365–384.

Ficken, K.J., Farrimond, P., 1995. Sedimentary lipid geochemistry of Framvaren: Impacts of a changing environment. Marine Chemistry 51, 31–43.

Frignani, M., Langone, L., 1991. Accumulation rates and $^{137}$Cs distribution in sediments off the Po River delta and the Emilia-Romagna coast (northwestern Adriatic Sea, Italy). Continental Shelf research 11, 525–542.

Frignani, M., Langone, L., Pacelli, M., Ravaioli, M., 1992. Input, distribution and accumulation of dolomite in sediments of the Middle Adriatic Sea. Rapports internationals Mer Mediterranee 33, 324.

Gibbs, Z., 2000. The origin of fine grained magnetite in sediments. Unpublished Ph.D. Thesis, University of Liverpool.

Guilizzoni, P., Oldfield, F. (Eds.), 1996. Palaeoenvironmental Analysis of Italian Crater Lake and Adriatic Sediments (PALICLAS). Memorie del'Istituto Italiano di Idrobiologia 55, 357pp.

Hemleben, C., Spindler, M., Anderson, O.R., 1989. Modern Planktic Foraminifera. Springer, New York.

Hounslow, M.W., Maher, B.A., 1996. Quantitative extraction and analysis of carriers of magnetization in sediments. Journal of Geophysics International 124, 57–74.

Jalut, G., Amat, A.E., Bonnet, L., Gauquelin, T., Fontugne, M., 2000. Holocene climatic changes in the Western Mediterranean, from south-east France to south-east Spain. Palaeogeography, Palaeoclimatology, Palaecology 160, 255–290.

Jorissen, F.J., 1988. Benthic Foraminifera from the Adriatic Sea; principles of phenotypic variation. Utrecht Micropal. Bulletin 37, 176.

King, J., Banerjee, S., Marvin, J., Ozdemir, O., 1982. A comparison of different magnetic methods for determining the relative grain size of magnetite in natural materials; some results from lake sediments. Earth and Planetary Science Letters 59, 404–419.

Kiriakouslakis, K., Stutt, E., Rowland, S.J., Vangriesheim, A., Lampitt, R.S., Wolff, G.A., 2001. Controls on the organic chemical composition of settling particles in the Northeast Atlantic ocean. Progress in oceanography 50, 65–87.

Langone, L., Asioli, A., Correggiari, A., Trincardi, F., 1996. Age-depth modeling through the late Quaternary deposits of the central Adriatic basin. In: Guilizzoni, P., Oldfield, F. (Eds.), Palaeoenvironmental Analysis of Italian Crater Lake and Adriatic Sediments (PALICLAS). Memorie del'Istituto Italiano di Idrobiologia 55, pp. 177–196.

Lees, J.A., Pethick, J.S., 1995. Problems associated with quantitative magnetic sourcing of sediments of the Scarborough to Mablethorpe coast, Northeast England, UK. Earth Surface processes and landforms 20, 795–806.

Lowe, J., Accorsi, C.A., Bandini-Mazzanti, M., Bishop, A., van der Kaars, S., Forlani, L., Mercuri, A.M., Rivalenti, C., Torri, P., Watson, C., 1996. Pollen stratigraphy of sediment sequences from lakes Albano and Nemi, (near Rome) and from the central Adriatic, spanning the interval from oxygen isotope stage 2 to the present day. In: Guilizzoni, P. and Oldfield, F. (Eds.), Palaeoenvironmental Analysis of Italian Crater lake and Adriatic Sediments (PALICLAS). Memorie del'Istituto Italiano di Idrobiologia 55, pp. 71–98.

Milliman, J.D., Syvitski, J.P.M., 1992. Geomorphic/tectonic control of sediment discharge to the ocean: the importance of small mountainous rivers. Journal of Geology 100, 525–544.

Misserochi, S., Faganeli, J., Balboni, V., Heussner, S., Monaco, A., Kerherve, P., 1998. Characteristics and sources of the settling particulate organic matter in the South Adriatic basin. Organic Geochemistry 30, 411–421.

Mozeti, P., Fonda Umani, S., Cataletto, B., Malej, A., 1998. Seasonal and inter-annual plankton variability in the Gulf of Trieste (northern Adriatic). ICES Journal of Marine Science 55, 711–722.

Müller, P.J., Kirst, G., Ruhland, G., von Storch, I., Rosell-Mélé, A., 1998. Calibration of alkenone paleotemperature index $U_{37}^{k'}$ based on core tops from the eastern South Atlantic and the global ocean (60°N–60°S). Geochimica et Cosmochimica Acta 62, 1757–1771.

Oldfield, F., 1994. Toward the discrimination of fine grained ferrimagnets by magnetic measurements in lake and near-shore marine sediments. Journal of Geophysical Research 99, 9045–9050.

Oldfield, F., Frignani, M., 1995. The magnetic properties of nine short cores from the North West Adriatic: a preliminary report. Proceedings of Workshop 3, Projetto Stragetico Clima, Ambiente e Territorio nel Mezzogiorno, Potenza, 1990, pp. 217–242.

Oldfield, F., Frignani, M., Yu, L., 1995. The magnetic properties of four sediment cores from the Adriatic: a preliminary report. Proceedings of Workshop 3, Projetto Stragetico Clima, Ambiente e Territorio nel Mezzogiorno, Potenza, 1990, pp. 681–701.

Pelejero, C., Grimalt, J.O., 1997. The correlation between the $U_{37}^{k'}$ index and sea surface temperatures in the warm boundary: The South China Sea. Geochimica et Cosmochimica Acta 62, 4789–4797.

Prahl, F.G., Wakeham, S.G., 1987. Calibration of unsaturation patterns in long-chain ketone compositions for palaeotemperature assessment. Nature 330, 367–369.

Ramrath, Antje, Sadori, Laura, and Negendank, Jörg F.W., 2000. Sediments from Lago di Mezzano, central Italy: a record of Lateglacial/Holocene climatic variations and anthropogenic impact. The Holocene 10, 87–95.

Rechka, J.A., Maxwell, J.R., 1988. Unusual long chain ketones of algal origin. Tetrahedron Letters 29, 2599–2600.

Rolph, T.C., Shaw, J., 1986. Variations of the geomagnetic field in Sicily. Journal of Geomagnetism and Geoelectricity 38, 1269–1277.

Rolph, T.C., Oldfield, F., Van der Post, K.D., 1996. Palaeomagnetism and rock-magnetism results from Lake Albano and the central Adriatic Sea (Italy). In: Guilizzoni, P. and Oldfield, F. (Eds.), Palaeoenvironmental Analysis of Italian Crater Lake and Adriatic Sediments (PALICLAS). Memorie del'Istituto Italiano di Idrobiologia 55, pp. 265–284.

Rosell-Mélé, A., Carter, J.F., Parry, A.T., Eglinton, G., 1995. Determination of the $U_{37}^{k}$ index in geological samples. Analytical Chemistry 67, 1283–1289.

Roveri, M., Asioli, A., Correggiari, A., Trincardi, F., 1998. Physical stratigraphy of the HST wedge of the Adriatic basin. Abstract Proceedings of the SEPM-IAS Research Conference "STRATCON 1998 Strata and sequences on shelves and slopes", Catania, Italy, 15–19 settembre 1998.

Siani, G., Paterne, M., Michel, E., Sulpizio, R., Sbrana, A., Arnold, M., Haddad, G., 2001. Mediterranean Sea Surface Radiocarbon Reservoir Age Changes Since the Last Glacial Maximum Science, 294, 1917–1920.

Sikes, E.L., Volkman, J.K., Robertson, L.G., Pichon, J.-J., 1997. Alkenones and alkenes in surface waters and sediments of the Southern Ocean: implications for palaeotemperature estimation in polar regions. Geochimica et Cosmochimica Acta 61, 1495–1505.

Sonzogni, C., Bard, E., Rostek, F., Lafont, R., Roselle-Melé, A., Eglinton, G., 1997. Core-top calibration of the alkenone index vs. sea surface temperature in the Indian Ocean. Deep-Sea Research II 44, 1445–1460.

Stuiver, M., Reimer, P.J., 1993. Extended $^{14}C$ data base and revised CALIB 3.0. $^{14}C$ age calibration program. Radiocarbon 35, 215–230.

Stuiver, M., Reimer, P.J., Bard, E., Beck, J.W., Burr, G.S., Hughen, K.A., Kromer, B., McCormac, F.G., v.d. Plicht, J., Spurk, M., 1998. INTCAL98 Radiocarbon age calibration 24,000–0 cal BP. Radiocarbon 40, 1041–1083.

Ternois, Y., Sicre, M.-A., Boireau, A., Conte, M.H., Eglinton, G., 1997. Evaluation of long-chain ketones as palaeo-temperature indicators in the Mediterranean Sea. Deep-Sea Research I 44, 271–286.

Trincardi, F., Correggiari, A., Roveri, M., 1994. Late Quaternary transgressive erosion and deposition in a modern epicontinental shelf: the Adriatic semi-encolsed basin. Geo-Marine Letters 14, 41–51.

Trincardi, F., Cattaneo, A., Asioli, A., Correggiari, A., Langone, L., 1996a. Stratigraphy of the late Quaternary deposits in the central Adriatic basin and the record of short term climatic events. In: Guilizzoni, P. and Oldfield, F. (Eds.), Palaeoenvironmental Analysis of Italian Crater lake and Adriatic Sediments (PALICLAS). Memorie del'Istituto Italiano di Idrobiologia 55, pp. 39–70.

Trincardi, F., Asioli, A., Cattaneo, A., Correggiari, A., Vigliotti, L., Accorsi, C.A., 1996b. Transgressive offshore deposits on the Central Adriatic shelf: architecture complexity and the record of the Younger Dryas short-term event. In: Late-Glacial and Early Holocene Climatic and Environmental Changes in Italy. IL. Quaternario Italian. Journal of Quaternary Sciences 9, 753–762.

Turney, C.S.M., 1998. Extraction of rhyolitic ash from minerogenic lake sediments. Journal of Paleolimnology 19, 199–206.

Turner, G.M., Thompson, R., 1981. Lake sediment record of geomagnetic secular variation in Britain during Holocene times. Geophysical Journal of the Royal Astronomical Society 65, 703–725.

Van der Zwaan, G.J., Jorissen, F.J., 1991. Biofacial patterns in river-induced shelf anoxia. In: Tyson, R.V., Pearson, T.H. (Eds.), Modern and Ancient Continental Shelf Anoxia, Vol. 58. Geological Society of London Special Publication, pp. 65–82.